

Biological sciences

Direction of flagellum beat propagation is controlled by proximal/distal outer dynein arm asymmetry

Beatrice Freya Lucy Edwards^{1,*}, Richard John Wheeler^{1,*,#}, Amy Rachel Barker^{1,*}, Flávia Fernandes Moreira-Leite¹, Keith Gull¹, Jack Daniel Sunter^{2,#}

¹ Sir William Dunn School of Pathology, University of Oxford, South Parks Road, Oxford, OX1 3RE, UK

² Department of Biological and Medical Sciences, Oxford Brookes University, Gypsy Lane, Oxford, OX3 0BP, UK

* Equal contribution

Corresponding authors: richard.wheeler@path.ox.ac.uk, jsunter@brookes.ac.uk

Keywords: flagellum, motility, outer dynein arm, intraflagellar transport, trypanosomatid

Abstract

The 9+2 axoneme structure of the motile flagellum/cilium is an iconic, apparently symmetrical cellular structure. Recently, asymmetries along the length of motile flagella have been identified in a number of organisms, typically in the inner and outer dynein arms. Flagellum beat waveforms are adapted for different functions. They may start either near the flagellar tip or near its base (and may be symmetrical or asymmetrical). We hypothesised that proximal/distal asymmetry in the molecular composition of the axoneme may control the site of waveform initiation and direction of waveform propagation. The unicellular eukaryotic pathogens *Trypanosoma brucei* and *Leishmania mexicana* often switch between tip-to-base and base-to-tip waveforms, making them ideal for analysis of this phenomenon. We show here that the proximal and distal portions of the flagellum contain distinct outer dynein arm docking complex heterodimers. This proximal/distal asymmetry is produced and maintained through growth by a concentration gradient of the proximal docking complex, generated by intraflagellar transport. Furthermore, this asymmetry is involved in regulating whether a tip-to-base or base-to-tip beat occurs, which is linked to a calcium-dependent switch. Our data show that the mechanism for generating proximal/distal flagellar asymmetry can control waveform initiation and propagation direction.

Significance statement

The motile flagellum/cilium is found across all eukaryotic life, and it performs critical functions in many organisms including humans. A fundamental requirement for a motile flagellum/cilium is that it must undergo the correct and appropriate waveform for its specific function. Much is known about the generation of asymmetry in flagellum movement, however it is unknown how a motile flagellum specifies where waves should start and whether waves should go from base-to-tip, or from tip-to-base. We show here that in two flagellum model organisms (the human parasites *Trypanosoma brucei* and *Leishmania mexicana*), differences in the outer dynein arms between the distal and proximal regions of the flagellum determine wave propagation direction, and are generated and maintained by the flagellum growth machinery.

\body

Introduction

Eukaryotic flagella/cilia are highly conserved cellular structures and play key roles as both sensory and motile organelles. Motile flagella/cilia undergo different waveforms necessary for their function: a symmetrical sinusoid or helical flagellar-type beat (human sperm), or an asymmetrical wafting ciliary-type beat (ciliated epithelia, *Chlamydomonas reinhardtii*). Many organisms can switch between asymmetric and symmetric waveforms(1–6), and this switch is typically mediated by calcium(4, 6–14). In addition to the waveform shape, waveform propagation direction can vary, and these two phenomena are distinct. *C. reinhardtii* and animal sperm flagella generally undergo base-to-tip waveforms, while other flagella normally undergo tip-to-base waveforms (including *Leishmania* and *Trypanosoma*)(15–17). Many flagella can switch the direction of waveform propagation, including *Leishmania* and the sperm of some animal species, to change the direction of swimming(16, 18–22). Like changes in waveform symmetry, switching of waveform direction is calcium mediated(18–21, 23, 24). Regardless of whether or not it can switch between waveforms, every flagellum/cilium must somehow specify where a waveform should start, and thus the direction in which it propagates.

The mechanism defining the point at which waveforms are initiated has been generally overlooked, possibly because the most popular model of flagellar waveform propagation, the geometric clutch model, suggests that flagellar beating can start spontaneously(25). Moreover, experimental evidence shows that the beat can initiate not only at the flagellar tip but also mid-flagellum in trypanosomatids(16). However, since the initiation point defines the direction of waveform

propagation (proximal initiation for base-to-tip, distal for tip-to-base), determining the mechanisms by which the position and direction of flagellar beat is initiated is critical to our understanding of waveform generation and switching.

Motor proteins in the inner and outer dynein arm complexes (IDAs, ODAs) are key to the generation and control of flagellar movement. The canonical view is the inner dynein arms generate and regulate the beat, while outer dynein arms provide the force to generate the final waveform(26). This view is predominantly derived from genetic evidence in *C. reinhardtii*: loss of IDAs (of which there are several classes) tends to alter waveform shape(27), while loss of ODAs reduces flagellar beat frequency with a small effect on waveform shape(27, 28). ODA defects are one of the main causes of primary ciliary dyskinesia (PCD) in humans(29), a recessive genetic disorder characterised by chronic pulmonary disease, randomisation of the left/right body axis and infertility. In *Trypanosoma brucei* loss of ODAs eliminates the tip-to-base flagellar beat, preventing forward motion of the parasite(15, 30). *C. reinhardtii* mutants lacking ODAs move more slowly and cannot swim backwards in response to stimulation with light(27, 28, 31).

In recent years studies have revealed that components of the IDAs and ODAs in several organisms are asymmetrically arranged along the length of the flagellum. IDA asymmetries have been identified in *C. reinhardtii*(32, 33), and ODA asymmetries occur in several model organisms. In humans, this asymmetry differs between cell types. In ciliated epithelia the outer arm dynein DNAH5 localises to the whole axoneme while DNAH9 and DNAH11 localise only to the distal axoneme(34–36); in contrast, in sperm DNAH5 localises to the proximal flagellar axoneme and DNAH9 to the whole axoneme(34). *C. reinhardtii* has one microtubule doublet with particularly strong proximal/distal asymmetry(32, 37), and this asymmetry appears to be at least partially due to proximal-only localisation of an ODA-associated complex including *ODA5* & *ODA10*(38, 39). The function of proximal/distal asymmetry of ODAs has not previously been analysed in any detail, however it appears important: in humans disruption of the asymmetric DNAH proteins is associated with defects in ciliary motility and primary ciliary dyskinesia(34–36). In *C. reinhardtii*, mutations in the proximal proteins *ODA5* & *ODA10* are associated with defects in swimming, but this phenotype is complicated by the additional roles of these proteins in ODA assembly(38, 39). How these IDA and ODA asymmetries are generated is also largely unknown.

We hypothesised that proximal/distal molecular asymmetries in the flagellum control where flagellum waveform starts, and so control beat propagation direction and contribute to the control of beat type. Since asymmetry has been observed in the IDAs of *C. reinhardtii*, and the ODAs in at least two model organisms, we examined the flagella of *T. brucei* and *Leishmania mexicana* for similar asymmetries. These organisms are well-characterised models for flagellar motility, and are capable of switching between tip-to-base and base-to-tip waveforms. There is some evidence of asymmetry between the proximal and distal regions of the flagellum in *T. brucei*(40), although the functional relevance of this is not yet clear. We show that in both organisms, the proximal and distal regions of the flagellum contain distinct ODA docking complexes (DCs), with an inherent asymmetry achieved early and maintained throughout flagellum growth. We demonstrate that this asymmetry is produced and maintained by an IFT-dependent concentration gradient of DC proteins, by retrograde transport of proximal DCs. Finally, we show that ODA proximal/distal asymmetry is involved in regulating whether a tip-to-base or base-to-tip beat occurs, likely *via* a calcium-dependent switch.

Results

We observed that the proximal and distal regions of the *T. brucei* axoneme are not identical by thin-section transmission electron microscopy (TEM). The *T. brucei* flagellum is laterally attached to the

cell for most of its length; therefore, most transverse cross-sections through the flagellum have an attached cross-section through the cell body. This architecture allows unambiguous identification of flagellar axoneme cross-sections as proximal or distal, based on the size and ultrastructure of the neighbouring cell body. Averaged electron density analysis of distal axoneme cross-sections showed a subtle difference in electron density in the outer dynein arm region between the proximal and distal regions of the axoneme (Figure 1A). By this unbiased analysis no other differences were detectable, however this does not exclude smaller proximal/distal differences in other structures.

We identified candidate proteins that may be responsible for this asymmetry using TrypTag, a project localising every protein encoded in the *T. brucei* genome(41). TrypTag identified several proteins with proximal- or distal-only axoneme localisations, including homologs of the ODA docking complex proteins DC1/ODA3 & DC2/ODA1 in *C. reinhardtii*, corresponding to CCDC151 & CCDC114 respectively in humans. One DC1 and one DC2 homolog (Tb927.5.1900 & Tb927.11.16090 respectively) localised to the distal part (approximately half) of the axoneme and a second DC1 and second DC2 homolog (Tb927.8.4400 & Tb927.7.5660 respectively) localised to the proximal part (Figure 1B), as determined by N-terminal tagging. We named these proteins pDC1 & pDC2 and dDC1 & dDC2, forming the proximal (pDC) and distal (dDC) docking complex pairs, respectively. Asymmetry is unlikely to be due to aberrant targeting since both C-terminal tagging and N-terminal tagging gave the same results (See SI Appendix, Figure S1A).

In...., DC1 and DC2 are predicted to form a coiled coil heterodimer and are mutually dependent for flagellar localisation and function(42, 43). *T. brucei* DC proteins are rich in predicted coiled coils (See SI Appendix, Figure S1B), therefore to test if each of the 4 DC proteins (pDC1, pDC2, dDC1, dDC2) are mutually dependent on their putative partner for correct localisation, we generated inducible RNAi cell lines targeting the open reading frame (ORF) of each DC gene. RNAi target sequences were selected ensuring they are not present elsewhere in the genome(44), and spurious knockdown of an incorrect DC protein is unlikely due to very low (<20%) protein sequence identity and no length of identical DNA sequence >11 nucleotides between any pair of DC proteins. For each RNAi cell line, we fluorescently tagged either the same gene or the expected heterodimer partner at the endogenous locus. In cell lines where the same gene was both tagged and targeted for RNAi, fluorescent signal of the tagged protein was undetectable after 72hr of RNAi induction, confirming effective RNAi knockdown at the protein level (See SI Appendix, Figure S1C, Table 1). When a given DC gene was targeted for RNAi knockdown in a cell line expressing a tagged copy of its putative partner, RNAi induction led to loss of fluorescence signal for the expected partner protein: tagged dDC2 was undetectable following dDC1 RNAi (and *vice versa*), and tagged pDC2 was undetectable following pDC1 RNAi (and *vice versa*) (Figure 1C, Table 1). Off-target effects of RNAi seem unlikely, as they would not be expected to generate these clear reciprocal phenotypes. Hence, the four *T. brucei* DC proteins likely make distinct distal (dDC1+dDC2) and proximal (pDC1+pDC2) heterodimers. We therefore focused further on one pDC and one dDC protein, pDC1 and dDC2 respectively.

To examine whether DC proteins performed their expected function of docking the ODAs to the axoneme, we tagged each of the outer arm dynein (OAD) heavy chains (OAD α and OAD β), and one inner arm dynein (IAD) heavy chain (IAD β) as a negative control, on the background of RNAi targeting either dDC2 or pDC1. Prior to RNAi induction, both OAD and IAD fluorescence signals extended along the entire flagellum. Induction of pDC1 RNAi for 72hr had no detectable effect on OAD or IAD fluorescent signal (Figure 1D), however induction of dDC2 RNAi for 72hr resulted in decrease of OAD (but not IAD) fluorescence signal in the distal \approx 25% of the flagellum (Figure 1D). The loss of ODAs from the distal axoneme only following dDC2 RNAi was confirmed using electron microscopy (Figure 1E).

To determine how ODAs remain attached to the proximal axoneme in the absence of pDC1 we tested whether loss of the proximal docking complex alters localisation of the distal docking complex and *vice versa*. We therefore tagged pDC1 and pDC2 on the background of dDC2 RNAi, and tagged dDC1 and dDC2 on the background of pDC1 RNAi. Following 72hr induction of dDC2 RNAi, the pDC1 and pDC2 signals remained proximal but extended along the flagellum to $\approx 75\%$ of the flagellum length (Figure 1F, S1D, Table 1), matching the length of the OAD signal upon dDC2 RNAi (Figure 1D, S1D). Following 72hr induction of pDC1 RNAi, the dDC1 and dDC2 fluorescence signals extended to cover the entire flagellum (Figure 1F, S1D), indicating that the distal docking complex can dock ODAs to the entire axoneme in the absence of the proximal docking complex. RNAi knockdown of dDC1 with tagged pDC1 or pDC2 and RNAi knockdown of pDC2 with tagged pDC1 or pDC2 confirmed this result (See SI Appendix, Figure S1F, Table 1). Importantly, axoneme asymmetry changed upon RNAi knockdown of components of the proximal or distal docking complexes, indicating that both of these docking complexes must be present to generate asymmetry.

While lengthways asymmetries along the flagellar axoneme have been observed in other organisms, the mechanism that generates this asymmetry is unknown. To address this issue, we considered critically a number of possible models: DCs may attach to an underlying asymmetry, such as another protein or tubulin modification (Model 1). This is unlikely, as knockdown of DC proteins altered the asymmetry (Figure 1D,F) and thus they cannot purely be clients to an existing asymmetry. Asymmetry may be derived from flagellum growth, with the proximal docking complex assembled early and the distal complex later (Model 2). This is not correct, as proximal/distal asymmetry was achieved early and maintained throughout flagellar growth (see below). We considered the possibility that asymmetry comes from information passed through the lateral attachment of the flagellum to the *T. brucei* cell body (Model 3). This is also unlikely, as knockdown of DC proteins caused asymmetry changes without affecting flagellum/cell body attachment (Figure 1D,F). Finally, asymmetry may be generated intrinsically in the flagellum, by tip structures or by intraflagellar transport (IFT) (Model 4). As docking complex asymmetry extends over the whole flagellum and the switching point occurs at the midpoint, asymmetry is unlikely due to direct interaction with the basal body or flagellum tip structures. However, the IFT system that assembles the axoneme could generate asymmetry by creating a proximal/distal concentration gradient of DCs.

To test and make predictions about the IFT model (Model 4) of asymmetry generation we built a quantitative agent-based model of docking complex binding, diffusion and IFT transport. The axoneme was simulated in 100 nm sections, and the proximal and distal heterodimers were simulated as single particles which diffuse along the flagellum, attach to and detach from the axoneme and may be transported by IFT. The key parameters which define the behaviour of the model are the probability of DC attachment (*on*), detachment (*off*), diffusion (*D*) to a neighbouring section, rate of transport by IFT (*T*), and quantity of DCs (*Q*) (Figure 2A). Conceptually, IFT transport of unbound DCs (either retrograde transport for the proximal DCs, anterograde transport for the distal DCs, or transport of both) could generate a concentration gradient which drives proximal/distal asymmetry. This assumes that unbound docking complexes diffuse freely along the axoneme when not transported by IFT and then bind to the next available site. Simulating IFT transport of proximal DCs, distal DCs or both DCs all generated proximal/distal asymmetry (Figure 2B).

Our experiments showed that the effect on distal docking complexes upon proximal complex knockdown and *vice versa* was different: on knockdown of pDCs, the dDCs extended along the entire flagellum, while pDCs were still excluded from part of the distal flagellum on dDC knockdown (Figure 1F). This suggested only one of proximal or distal DCs are transported. We used this to constrain our model by specifying whether one or both DCs were transported by IFT and then simulating the

resulting flagellum asymmetry in the presence of either both DCs, just proximal DCs or just distal DCs, with the latter two mirroring the RNAi experiments (Figure 2B). Simulation of retrograde transport of the proximal docking complex alone matched the changes to docking complex localisation on RNAi knockdown. Any anterograde transport of distal docking complexes prevented the distal docking complex extending along the proximal flagellum in the absence of the proximal complex (Figure 2B cf. Figure 1F). Finally, given retrograde transport of the proximal docking complex, a higher binding affinity of pDC was necessary for the simulation to match the observed DC localisation (Figure 2C cf. Figure 1B). The model gave qualitatively similar results even with large changes to the estimated parameters (See SI Appendix, Figure S3A). Therefore our data is consistent with an asymmetry generation model whereby the higher affinity proximal docking complex is restricted to the proximal axoneme by retrograde IFT transport, while the lower affinity distal docking complex fills the remaining axoneme binding sites.

The IFT-mediated asymmetry model predicts that growing flagella will maintain their proximal distal asymmetry independent of flagellum length (Figure 2D). *T. brucei* grows a new flagellum each cell cycle, with each daughter cell inheriting one full-length flagellum. The new growing flagellum is always positioned anterior of the old flagellum(45, 46). Using a cell line in which dDC2 and pDC1 were each tagged with different fluorescent proteins, we saw that the new growing flagellum contained similar proportions of proximal pDC1 and distal dDC2 to those found in the old flagellum (Figure 2D). Measurements of the dDC2 signal length confirmed that there was no correlation between flagellum length and the proportion of the flagellum with dDC2 signal (Spearman's rank correlation -0.013, $n=123$) (Figure 2D). Therefore the DC asymmetry is established early during flagellum growth, eliminating flagellum growth *per se* as a mechanism of asymmetry generation.

The IFT model also predicts that new distal docking complex molecules would be incorporated at the distal end of growing flagella. In contrast, the proximal docking complex would be incorporated more slowly and diffusely, weakly focused at the distal end of the proximal docking complex region, which corresponds to the middle of the flagellum (Figure 2E). We tested this prediction using pulse labelling in cell lines expressing dDC2 or pDC1 tagged with HaloTag (See SI Appendix, Figure S2B). Incubation with a non-fluorescent ligand followed by a pulse with fluorescent ligand allowed us to observe the incorporation of new material into the flagellum; as predicted by the model, new dDC2 was incorporated at the distal end of new growing flagella and new pDC1 signal was weaker, focused towards the middle of growing flagella (Figure 2E).

Finally, the IFT model predicts disruption of IFT should alter the proximal/distal asymmetry of the flagellum. The precise effect is hard to predict: IFT disruption also reduces flagellum growth and IFT-mediated entry of docking complexes into the flagellum may be affected. The model suggests that the proximal docking complex is unlikely to require IFT to enter the flagellum, as it is actively removed by retrograde transport, while the distal docking complex may require IFT to enter the flagellum and so be depleted on IFT disruption. Simulation predicts reduced IFT will allow the pDC region to extend distally, outcompeting the binding of dDC, and this effect could be exacerbated by a reduction in the quantity of distal docking complex proteins. We tested this prediction using RNAi knockdown of IFT46 (Tb927.6.3100), which is required for anterograde IFT, thus disrupting both anterograde and retrograde IFT. Induction of IFT46 RNAi for 24 h caused the cellular phenotypes of IFT knockdown(47): cells with shorter flagella, cytokinesis defects, and reduced population growth (See SI Appendix, Figure S2C). We tagged dDC2 and pDC1 with different fluorescent proteins in this RNAi cell line, and then looked at cells 8 h and 16 h after RNAi induction to examine the earliest effects of IFT46 RNAi. In a minority of dividing cells at 8 h and a majority at 16 h the new flagellum had the predicted changes to axoneme asymmetry. The region occupied by pDC1 was greatly expanded, with a corresponding

reduction in dDC2 signal (Figure 2F, Table 1). This reduced proportion of dDC2 signal was inherited by one daughter cell and after 24 h induction cells with a single flagellum and a similar proximal/distal defect were common in the population (See SI Appendix, Figure S2D). This confirms that retrograde transport of proximal docking complexes generates a concentration gradient which, combined with different dissociation rates of pDC and dDC, generates the observed asymmetry in docking complexes.

As outer dynein arms are required for flagellar beating, we reasoned there may be regulatory proteins for modulating the site of waveform initiation (and therefore waveform propagation direction) which bind only to either the proximal or distal ODAs. Using TrypTag(41), we identified a candidate beat regulation protein (Tb927.9.4420) based on its localisation and predicted domains. It is the only EF-hand/calmodulin-domain containing protein (Figure 3A) localised specifically to the distal axoneme (Figure 3B). This protein could plausibly interact with Ca^{2+} , a known beat regulator. The most similar *C. reinhardtii* protein is LC4 (but LC4 is not a reciprocal best BLAST result), an outer dynein arm-binding protein implicated in flagellar beat control(48, 49). We named this protein LC4-like. Fluorescently tagged LC4-like localised to the distal axoneme, similar to dDC1/dDC2, and the fluorescence signal was undetectable following induction of dDC2 RNAi knockdown for 72hr, suggesting that LC4-like relies upon the distal docking complex for localisation (Figure 3B, Table 2). These results provide further support for the biological plausibility of LC4-like as a distal ODA regulator. LC4-like is not an obligate part of the docking complex, as 72hr induction of LC4-like RNAi knockdown did not affect the localisation of dDC2 (Figure 3B, Table 2). This is similar to *C. reinhardtii*, where the docking complex heterodimer is associated with a calcium-binding protein, DC3 (*ODA14*)(50); however, we did not find a clear homologue of DC3 by reciprocal best BLAST in *T. brucei*. RNAi knockdown of pDC1 caused the LC4-like signal to extend to the proximal end of the flagellum (Figure 3C, Table 2), as does the distal docking complex. In *C. reinhardtii* LC4 binds the ODAs(49), and therefore LC4-like may only bind to ODAs attached by the distal docking complex, although it may bind directly to the dDCs.

We predicted that disruption of proximal/distal asymmetry or LC4-like would alter the direction of flagellum waveform propagation. However, full analysis of flagellar waveforms is complicated in *T. brucei* due to the lateral attachment of the flagellum to the cell body. To better analyse changes in flagellum movement we used the related parasite *L. mexicana*, which does not have a laterally attached flagellum, greatly simplifying the beat waveform analysis. We identified *L. mexicana* homologs of dDC1, dDC2, pDC1 and pDC2 (LmxM.10.0960, LmxM.31.2900, LmxM.15.0540 and LmxM.06.1040 respectively). Each has comparable localisations to those in *T. brucei*, except that the proximal docking complex occupies $\approx 20\%$ of the proximal axoneme rather than 50% (See SI Appendix, Figure S3A). Deletion of both alleles of dDC2 on the background of fluorescently tagged pDC1 caused distal extension of the pDC1 signal and loss of ODAs from the distal axoneme, similar to dDC2 RNAi knockdown in *T. brucei* (See SI Appendix, Figure S3B,C cf. Figure 1E,F). The localisation of LC4-like (LmxM.01.0620) in *L. mexicana* also reflected that of *T. brucei* and deletion of both dDC2 alleles caused loss of LC4-like from the axoneme, similar to dDC2 RNAi knockdown in *T. brucei* (See SI Appendix, Figure S3D cf. Figure 3B).

Deletion of both alleles of *L. mexicana* dDC2 decreased the speed, velocity and directionality of cell swimming (Figure 4A), though flagella still moved. We analysed flagellum movement with 200 Hz high framerate video microscopy. *L. mexicana* can undergo both a tip-to-base sinusoidal flagellar beat and a base-to-tip asymmetric ciliary type flagellar beat(16). Normal flagellum movement in the parental cell line was mostly a flagellar beat, with occasional pauses or ciliary beats, and a large minority of cells undergoing low-frequency or uncoordinated movement (Figure 4B, Video 1). Flagellum movement after dDC2 deletion entirely lacked flagellar beats. Approximately half of flagella were uncoordinated and half of cells underwent an asymmetric base-to-tip reverse beat, far more than in

the parental cell line (Figure 4C,D, Video 1). The shape of base-to-tip waveforms was unaffected, with the same asymmetric shape as the parental cell line. The distal ODAs are therefore required for the tip-to-base flagellar beat to occur, most likely by initiating the flagellar beat waveform at the distal end.

Deletion of both LC4-like alleles caused a significant increase in swimming speed and velocity (Figure 4A). High frame rate video of the LC4-like deletion showed that flagellum movement was almost entirely a flagellar beat, with fewer pauses in the beat, less uncoordinated movement and far fewer ciliary beats than in the parental cell line (Figure 4B, Video 1). The frequency of the flagellar beat was also significantly higher in the LC4-like deletion (44.2 ± 8.9 Hz, $n=33$) than in the parental cell line (25.4 ± 9.0 Hz $n=27$) (Mann-Whitney U test $p < 10^{-10}$), although the waveform showed the same sinusoidal shape. LC4-like therefore appears to be a regulatory protein that inhibits the initiation of flagellar beat waveforms, and the absence of LC4-like has the opposite effect to that of missing distal outer dynein arms.

Discussion

It is becoming increasingly apparent that there are molecular asymmetries in the IDAs and ODAs of the axoneme both between the outer microtubule doublets(51, 52) and along the length of the axoneme(32–34, 36) in many organisms. In *C. reinhardtii*, proximal/distal and doublet-doublet asymmetries in the IDAs have been implicated in controlling whether a flagellum waveform is asymmetric or symmetrical(27). We show here that proximal/distal axoneme asymmetry is also important in controlling the site of flagellum waveform initiation and therefore the direction of waveform propagation. The control of the site of waveform initiation and the control of waveform asymmetry are significantly different phenomena; however, as both involve proximal/distal asymmetries in dynein arms, there may be similarities in the underlying mechanisms.

We have concentrated on the lengthwise axonemal asymmetry and demonstrate that both *T. brucei* and *L. mexicana* use distinct proximal and distal docking complexes to confer proximal/distal asymmetry of the molecular composition of ODAs in the axoneme. The resulting axoneme structure is similar to previous reports of asymmetry of outer arm dyneins in human cilia and sperm flagella(34–36), and to proximal/distal asymmetry of one axoneme microtubule doublet in *C. reinhardtii*(32, 37), which is linked to docking complex-related accessory proteins(38, 39). It is perhaps surprising that we identified the ODAs, rather than IDAs, as important for specifying the site of waveform initiation in *T. brucei* and *L. mexicana*. The canonical view (based primarily on *C. reinhardtii*) is that ODAs provide the force which drives the beat, while the IDAs initiate and regulate the waveform shape(26). However, we saw no clear proximal/distal asymmetry of IDAs by TEM in *T. brucei*, while loss of distal ODA DCs or the ODA-associated LC4-like was sufficient to change the site of waveform initiation. The change in the site of waveform initiation occurred with the normal waveform for tip-to-base (symmetric) and base-to-tip (asymmetric) waveforms. This is consistent with IDAs regulating the shape of the waveform (as in *C. reinhardtii*) but ODAs regulating the site of wave initiation. While we cannot formally exclude a parallel or underlying role of IDAs in controlling whether waveform initiation is distal or proximal, we saw no change in the localisation of IDA components during docking complex knockdown. However, as *C. reinhardtii* flagella always undergoes base-to-tip waveforms, it is also possible *C. reinhardtii* has lost some proximal/distal ODA asymmetries. Given this asymmetry occurs in diverse organisms, proximal/distal asymmetry in ODAs may represent a general mechanism for defining proximal and distal regions of the flagellum, although the specific proteins involved may differ through evolution. Guided by this, we identified a similar, previously unrecognised, phenomenon by analysing previously published data from the unrelated unicellular parasite *Giardia lamblia*(53). We

noticed that this species also has proximal and distal DC1-like proteins (GL50803_13288 & GL50803_16998) but a single DC2 (GL50803_114462).

Proximal/distal axoneme asymmetry had been described, but the mechanism of asymmetry generation was unknown, although competition for axoneme binding between distal and proximal components has been suggested for *C. reinhardtii* and *T. brucei*(33, 40). We show that asymmetry of the docking complexes is generated at the very earliest stages of flagellar growth and maintained as the flagellum elongates. Therefore the mechanism by which asymmetry is generated is intrinsic to the flagellar growth machinery. By modelling various permutations of the IFT transport of each docking complex, and comparing these with the experimental data, we show that two factors are sufficient to generate the asymmetries we observed: lower-affinity binding of the distal docking complex and retrograde transport of the proximal docking complex by IFT. Retrograde transport of the proximal docking complex toward the base of the flagellum generates and maintains a concentration gradient of the proximal docking complex. The higher affinity of the proximal docking complex out-competes binding of the distal docking complex, generating the axoneme asymmetry, and unbound distal docking complex is free to diffuse throughout the flagellum and fills in the remaining spaces. This model is simple, and in reality there are likely to be additional complexities, yet it precisely matches our experimental observations: i) maintenance of asymmetry throughout flagellar growth, ii) the locations at which newly synthesised proximal and distal docking complexes are incorporated into the growing flagellum, and iii) the effects on docking complex distribution when IFT is disrupted.

Diffusion of docking complexes along the axoneme, filling available binding sites, has previously been observed in *C. reinhardtii* flagella lacking ODAs; the docking complex enters the base of the flagellum, binds first to the proximal axoneme and proceeds distally, filling each unoccupied site(54). Some evidence for diffusion of the ODA protein DNAI1 has also been observed in *T. brucei*(55). Diffusion alone could initially generate a proximal/distal axoneme asymmetry; for example, diffusion of a limited quantity of high-affinity proximal docking complex into the proximal flagellum out-competes a low-affinity distal docking complex. However, our simulation indicated retrograde transport of the proximal complex by IFT was required to maintain this asymmetry over an extended period. Together, our data indicates a concentration gradient generated by directional transport of a protein complex can generate and maintain asymmetry in an organelle, and may be a fundamental mechanism through which an organelle can generate internal asymmetry/structure, analogous to the concentration gradients driving polarity in cell and tissue development.

We show that proximal/distal asymmetry of ODAs in *T. brucei* and *L. mexicana* is involved in the control of the site of initiation of flagellum beat waveforms. Loss of the distal docking complex resulted in loss of ODAs from only the distal portion of the flagellum, and the subsequent loss of tip-to-base waveforms demonstrates that ODAs in this region are required for initiation and/or propagation of tip-to-base waveforms. This is consistent with previous studies showing that beat initiation occurs in the most distal 2 μm of the flagellum(16). Proteins involved in regulating waveform shape are often associated with the ODAs, with LC1 and LC4 representing well-characterised examples in *C. reinhardtii*(48, 49, 56), though IDA components are also important. In *T. brucei*, knockdown of the ODA component LC1 resulted in loss of tip-to-base waveform generation(15, 29), but this was complicated by the complete loss of ODAs in these mutants. Our data showed a distal only LC4-like protein, with a Ca^{2+} binding site, is a repressor of distal initiation of tip-to-base waveforms. This reveals that the distal ODAs are an important site for the regulation of initiation of flagellar waveforms, thus controlling whether the waveform travels tip-to-base or base-to-tip.

Flagellum movement arises from dynein-driven sliding of neighbouring axoneme microtubule doublets(57) and there are three different models to explain waveform propagation(57). The leading

model is arguably the geometric clutch hypothesis, which states that mechanical distortion of the axoneme as it bends regulates force generation by regulating dynein arm engagement(25, 58, 59). The simplest interpretation of our results in the context of this hypothesis is that the distal docking complex positions the distal ODAs so they are more likely than the proximal ODAs to spontaneously engage and start a flagellar waveform (although more complex interpretations, like involvement of the IDAs, are also possible). Loss of distal ODAs prevents distal waveform initiation, allowing spontaneous proximal initiation. Calcium binding to LC4-like could then modulate the likelihood of engagement of the distal ODAs, regulating the site of waveform initiation and, therefore, the direction of beat propagation. This role for LC4-like is consistent with previous data in *C. reinhardtii*, where the switch from flagellar to ciliary beating upon photostimulation is calcium-mediated(7, 60).

Given that mutations both in docking complexes(61) and in proteins with an asymmetric localisation(36) lead to primary ciliary dyskinesia in humans, a better understanding of the mechanisms by which asymmetry occurs and how it contributes to flagellar motility is essential. Here, we demonstrate that molecular asymmetries within the axoneme can be generated by an IFT-dependent concentration gradient of proteins within the flagellum and that this asymmetry is linked to the control of waveform initiation, defining whether a tip-to-base or base-to-tip beat occurs. This control is mediated by a potentially calcium-responsive protein, which relies on the distal docking complexes for proper localisation, enabling *T. brucei* and *L. mexicana* parasites to switch flagellum waveform propagation direction and control their swimming. It seems likely that proximal/distal asymmetry is a common feature of cilia and flagella, and that the true extent and function of this important phenomenon are only just beginning to become clear.

Methods

SmOxP9 procyclic *T. brucei* (derived from TREU 927, expressing T7 RNA polymerase and tetracycline repressor(62)) were grown in SDM79 with 10% FCS(63). Constructs for endogenous mNeonGreen (mNG) or mScarlet mSc tagging were generated by PCR and transfected as previously described(64), with the pPOT version 4 series of vectors used as PCR templates(64), specifically pPOT mNG Blast or pPOT mSc Neomycin. Target sequences were selected and primers were designed using TAGit (<http://www.sdeanresearch.com/cgi-bin/tagitA.cgi>)(64) (See SI Appendix, Table S1). Constructs for RNAi were generated using the pQuadra system(65). Primers for amplification of the target ORF fragment were designed using RNAit (<http://trypanofan.path.cam.ac.uk/software/RNAit.html>). Transfectants were selected with the necessary combination of 5 µg/ml blasticidin S hydrochloride, 5 µg/ml G-418 disulfate, and 10 µg/ml phleomycin and cloned by limiting dilution in 96 well plates.

Cas9T7 *L. mexicana* (derived from WHO strain MNYC/BZ/62/M379, expressing Cas9 and T7 RNA polymerase(66)) were grown in M199 supplemented with 2.2 g/l NaHCO₃, 0.005% haemin, 40 mM HEPES-HCL pH 7.4 and 10% FCS. Constructs and sgRNA templates for endogenous mNG tagging templates were generated by PCR as previously described(66) and transfected as previously described(64). The pLrPOT series of vectors were used as PCR templates for generating tagging constructs, specifically pLrPOT mNG Blast. These are a variant of pLPOT(64) with *T. brucei* and *Crithidia fasciculata* 5' or 3' untranslated regions (UTRs) and intergenic sequences replaced with complete *L. mexicana* intergenic sequences. The *T. brucei* actin 5' UTR was replaced with the *L. mexicana* actin (LmxM.04.1230) 5' UTR, the *T. brucei* aldolase 3' UTR/*C. fasciculata* PGKB 5' UTR fusion was replaced with the *L. mexicana* histone 2B intergenic sequence (between LmxM.19.0050 and LmxM.19.0030), the *C. fasciculata* PGKA/B intergenic was replaced with the *L. mexicana* histone 2A intergenic (between LmxM.08_29.1740 and LmxM.08_29.1730) and the *T. brucei* aldolase 3' UTR was replaced with the *L. mexicana* eukaryotic initiation factor 5 (LmxM.25.0720) 3' UTR. Constructs and sgRNA templates for open reading frame deletion were generated by PCR and transfected as previously described, using

pT Blast and pT Neo as templates(66). Primers were designed using LeishGEdit (<http://www.LeishGEdit.net>)(66). Transfectants were selected with the necessary combination of 20 µg/ml puromycin dihydrochloride, 5 µg/ml blasticidin S hydrochloride, 40 µg/ml G-418 disulfate, 50 µg/ml nourseothricin sulfate and 25 µg/ml phleomycin and cloned by limiting dilution in 96 well plates using MM199 as previously described(64).

T. brucei and *L. mexicana* cultures were grown at 28°C. Culture density was maintained between 1×10^6 (*T. brucei*) or 1×10^5 (*L. mexicana*) and 1×10^7 cells/ml for continued exponential population growth. Culture density was measured using a CASY model TT cell counter (Roche Diagnostics) with a 60 µm capillary.

T. brucei and *L. mexicana* cell lines expressing fluorescent fusion proteins were imaged live. Cells were washed three times by centrifugation at 800 g followed by resuspension in vPBS (PBS supplemented with 10 mM glucose and 46 mM sucrose). DNA was stained by including 10 µg/ml Hoechst 33342 in the second wash. Washed cells were settled on glass slides then immediately observed. To generate cytoskeletons, cells were prepared as for live cell microscopy, the membrane solubilised with 0.5% NP40 in PEME (100 mM PIPES-NaOH pH 6.9, 2 mM EGTA, 1 mM MgSO₄ and 100 nM EDTA) for 30 s, then the remaining cytoskeleton fixed by immersion in -20°C methanol for 20 min. Cytoskeletons were then rehydrated in PBS, mounted in 50 mM phosphate-buffered glycerol pH 8.0 and imaged. For fluorescent labelling of HaloTag fusion proteins cells were incubated in culture with fluorophore-conjugated ligands. For labelling of all HaloTag fusion protein, cells were incubated with TMRDirect ligand (Promega) at 0.1 µM final concentration for 45 min. For pulse labelling of HaloTag fusion protein, cells were incubated with Coumarin ligand (Promega) at 10 µM final concentration for 45 min, washed three times with medium, then incubated with 0.1 µM TMRDirect (tetramethylrhodamine) ligand for 45 min. We could not detect the expected blue fluorescence of the Coumarin ligand, but found it was an effective block, as described previously(67). Widefield epifluorescence and phase contrast images were captured using a Zeiss Axioimager.Z2 microscope with a 63× NA 1.40 oil immersion objective and a Hamamatsu ORCA-Flash4.0 camera. Cell morphology measurements were made in ImageJ(68).

Swimming and flagellar beat behaviours were analysed for cells in exponential growth in normal culture medium essentially as previously described(17). For cell swimming analysis, a 25.6 s video at 5 frames per second under darkfield illumination was captured from 5 µl cell culture in a 250 µm deep chamber using a Zeiss Axioimager.Z2 microscope with 10× NA 0.3 objective and a Hamamatsu ORCA-Flash4.0 camera. Particle tracks were traced automatically, and mean cell speed, mean cell velocity and cell directionality (the ratio of velocity to speed) were calculated as previously described(17). For flagellar beat analysis, a 4 s video at 200 frames per second under phase contrast illumination was captured from a thin film of cell culture between a slide and coverslip using a Zeiss Axiovert.A1 microscope with a 20× NA 0.3 objective and an Andor Neo 5.5 camera. Unlike previously, glass slides and coverslips were blocked with bovine serum albumen (BSA) to reduce cell adhesion to the glass, by immersion in 1% BSA for 60 s then washed with water and allowed to dry prior to use. Flagellar beat behaviours for each cell in the 4 s videos were classified manually.

Thin-section transmission electron microscopy samples were prepared as previously described(69, 70). Sections with nominal thicknesses between 70 nm were cut, stained with lead citrate, and then observed using an FEI Tecnai 12 TEM with a Gatan Ultrascan 1,000 CCD camera. Transverse sections through flagella were classified into proximal or distal based on the width of the cell body to which the flagellum was attached: proximal if the cell body was over ≈500 nm wide, and distal if under ≈500 nm or if the flagellum was not laterally attached to a cell. Ninefold rotational averages of the axoneme structure (Markham rotations) were generated following perspective correction to ensure a

circular axoneme cross-section as previously described(71–73). Axoneme cross-sections were pooled from negative controls from previous studies, then were stacked and averaged in ImageJ(68) to generate average proximal and distal axoneme electron density.

The agent-based simulation of flagellum assembly and DC proximal/distal asymmetry was written in Javascript/NodeJS. pDC and dDC complexes were simulated as two particles, and particles could either be attached at a fixed position in the axoneme or detached and free to diffuse. The flagellum was simulated in discrete bins from proximal to distal (segments) and in discrete time steps (intervals). An evaluation interval of 0.1 s and a flagellum segment size of 100 nm were selected for useful granularity of binding/dissociation events and axoneme binding capacity for DCs. DC binding capacity of the axoneme was 37 /segment, assuming ninefold axoneme symmetry and a 24 nm repeat of outer dynein arms(74). Probability of detached DC diffusion to an adjacent segment was 0.436 /interval, calculated from the probability of diffusing 1 segment distance in 1 interval assuming a 5 nm docking complex effective hydrodynamic radius and a flagellar cytoplasm viscosity 670× greater than water (derived from BioNumbers(75) ID 108250, the diffusion constant of GFP in water, and the diffusion of rate of GFP in bacterial cytoplasm(76)). Diffusion occurs equally in both directions, therefore probability of anterograde diffusion and retrograde diffusion (D) were both 0.208 /interval. Probability of DC binding to a free site in the axoneme (on) was set to 1, assuming binding kinetics are fast relative to dissociation and diffusion. Probability of dissociation (off) was initially set to 4×10^{-5} , giving a dissociation half-life on the order of 1 h. Flagellum growth rate was constant and set to 10 $\mu\text{m}/\text{h}$, up to a maximum length of 23 μm (77). Quantity of docking complex protein (Q) is expressed as a factor excess over the number of binding sites in half of the flagellum and was initially set to 2.0. For example $Q_{dist}=Q_{prox}=1$ indicates an equal number of DC particles and axoneme binding sites, half pDC and half dDC. $Q_{dist}=Q_{prox}=2.0$ indicates a 100% excess. In every interval in which flagellum growth led to addition of a new axoneme segment the necessary number of new detached pDC and dDC particles were added to the base of the flagellum. IFT was simulated by sweeping from proximal to distal (anterograde transport) or distal to proximal (retrograde transport) and moving the first detached dDC (for anterograde) or pDC (for retrograde) particle encountered to the distal or proximal end of the axoneme respectively. Quantity of IFT (T) was initially set to 0.2 /interval, assuming around 5 IFT trains per second(78) with one binding site per train. Dissociation probabilities were simulated with the following values: $off_{dist}=off_{prox}=4 \times 10^{-5}$, $off_{dist}=1 \times 10^{-5}$ $off_{prox}=1.6 \times 10^{-4}$, and $off_{dist}=1.6 \times 10^{-4}$ $off_{prox}=1 \times 10^{-5}$. The final values were $off_{dist}=1.6 \times 10^{-4}$ $off_{prox}=1 \times 10^{-5}$. pDC or dDC knockdowns were simulated with Q_{prox} , Q_{dist} , T_{prox} and T_{dist} as indicated in the text. The final values were $Q_{dist}=Q_{prox}=2.0$ and $T_{prox}=0.2$ and $T_{dist}=0.0$.

The localisations of the *T. brucei* docking complex proteins were initially identified from TrypTag.org(41). *T. brucei* and *L. mexicana* protein and genome sequences were accessed using TriTrypDB.org(79). *L. mexicana* orthologs of *T. brucei* proteins were identified using synteny and orthogroup data from TriTrypDB.org(79), and manually confirmed by reciprocal best BLAST. *C. reinhardtii*, *G. lamblia* and human orthologs were identified using orthogroups as found by orthofinder(80) run on 45 diverse eukaryote genomes, then manually checked by BLAST search. We used the same set of 45 ciliated and non-ciliated organism genomes as in previous studies concerning evolution of flagellar/ciliary components(81). Coiled coils were predicted using Coils v2.2 with default parameters(82). Key residues in the EF-hand fold were derived from Superfamily v1.75 (supfam.org)(83), specifically 1a03 A (S100 protein set) for SSF47473, and visualised using WebLogo(84).

Acknowledgements

We would like to thank Heather Jeffrey and Eva Gluenz for generating the *L. mexicana* LC4-like deletion cell line, Helen Farr and Emily Poon for contributing EM images and Catherine McEnhill for contributing to flagellum beat data collection. We would especially like to thank Samuel Dean and the other co-PIs of TrypTag. This work was supported by the Wellcome trust [103261/Z/13/Z, 108445/Z/15/Z, 104627/Z/14/Z].

Author contributions

JDS, RJW & KG designed and directed the research project. BE performed preliminary experiments. BFLE, JDS & ARB generated and analysed *T. brucei* cell lines. RJW generated and analysed *L. mexicana* cell lines. FML performed electron microscopy. ARB and JDS developed asymmetry mechanism experiments, RJW simulated the asymmetry mechanism. BFLE & RJW analysed cell swimming and flagellar beats. All authors contributed to data analysis and drafting the manuscript.

References

1. Ringo DL (1967) Flagellar Motion and Fine Structure of the Flagellar Apparatus in Chlamydomonas. *J Cell Biol* 33(3):543–571.
2. Ueki N, Matsunaga S, Inouye I, Hallmann A (2010) How 5000 independent rowers coordinate their strokes in order to row into the sunlight: Phototaxis in the multicellular green alga Volvox. *BMC Biol* 8:103.
3. Holwill MEJ (1966) The Motion of Euglena Viridis: The Role of Flagella. *J Exp Biol* 44(3):579–588.
4. Diehn B, Fonseca JR, Jahn TL (1975) High Speed Cinemicrography of the Direct Photophobic Response of Euglena and the Mechanism of Negative Phototaxis. *J Protozool* 22(4):492–494.
5. Kung C, Chang SY, Satow Y, Houten JV, Hansma H (1975) Genetic dissection of behavior in paramecium. *Science* 188(4191):898–904.
6. Naitoh Y (1968) Ionic Control of the Reversal Response of Cilia in Paramecium caudatum. *J Gen Physiol* 51(1):85–103.
7. Bessen M, Fay RB, Witman GB (1980) Calcium control of waveform in isolated flagellar axonemes of chlamydomonas. *J Cell Biol* 86(2):446–455.
8. Hyams JS, Borisy GG (1975) Flagellar coordination in Chlamydomonas reinhardtii: isolation and reactivation of the flagellar apparatus. *Science* 189(4206):891–893.
9. Schmidt JA, Eckert R (1976) Calcium couples flagellar reversal to photostimulation in Chlamydomonas reinhardtii. *Nature* 262(5570):713–715.
10. Hyams JS, Borisy GG (1978) Isolated flagellar apparatus of Chlamydomonas: characterization of forward swimming and alteration of waveform and reversal of motion by calcium ions in vitro. *J Cell Sci* 33(1):235–253.
11. Doughty MJ, Diehn B (1979) Photosensory transduction in the flagellated alga, Euglena gracilis I. Action of divalent cations, Ca²⁺ antagonists and Ca²⁺ ionophore on motility and photobehavior. *Biochim Biophys Acta* 588(1):148–168.
12. Iwade Y (2003) Photolysis of caged calcium in cilia induces ciliary reversal in Paramecium caudatum. *J Exp Biol* 206(7):1163–1170.
13. Iwade Y, Nakaoka Y (2008) Calcium regulates independently ciliary beat and cell contraction in Paramecium cells. *Cell Calcium* 44(2):169–179.
14. Shiba K, Inaba K (2017) Inverse relationship of Ca²⁺-dependent flagellar response between animal sperm and prasinophyte algae. *J Plant Res* 130(3):465–473.
15. Baron DM, Kabututu ZP, Hill KL (2007) Stuck in reverse: loss of LC1 in Trypanosoma brucei disrupts outer dynein arms and leads to reverse flagellar beat and backward movement. *J Cell Sci* 120(Pt 9):1513–1520.
16. Gadelha C, Wickstead B, Gull K (2007) Flagellar and ciliary beating in trypanosome motility. *Cell Motil Cytoskeleton* 64(8):629–643.
17. Wheeler RJ (2017) Use of chiral cell shape to ensure highly directional swimming in trypanosomes. *PLoS Comput Biol* 13(1):e1005353.
18. Shiba K, Shibata D, Inaba K (2014) Autonomous changes in the swimming direction of sperm in the gastropod Strombus luhuanus. *J Exp Biol* 217(6):986–996.
19. Holwill MEJ, McGregor JL (1975) Control of flagellar wave movement in Crithidia oncopelti. *Nature* 255(5504):157–158.

20. Johnston DN, Silvester NR, Holwill MEJ (1979) An Analysis of the Shape and Propagation of Waves on the Flagellum of Crithidia Oncopelti. *J Exp Biol* 80(1):299–315.
21. Sugrue P, Hirons MR, Adam JU, Holwill ME (1988) Flagellar wave reversal in the kinetoplastid flagellate Crithidia oncopelti. *Biol Cell Auspices Eur Cell Biol Organ* 63(2):127–131.
22. Yang Y, Lu X (2011) Drosophila Sperm Motility in the Reproductive Tract. *Biol Reprod* 84(5):1005–1015.
23. Mukhopadhyay AG, Dey CS (2016) Reactivation of flagellar motility in demembranated Leishmania reveals role of cAMP in flagellar wave reversal to ciliary waveform. *Sci Rep* 6:37308.
24. Mukhopadhyay AG, Dey CS (2017) Role of calmodulin and calcineurin in regulating flagellar motility and wave polarity in Leishmania. *Parasitol Res*:1–8.
25. Lindemann CB (1994) A “Geometric Clutch” Hypothesis to Explain Oscillations of the Axoneme of Cilia and Flagella. *J Theor Biol* 168(2):175–189.
26. Brokaw CJ (1994) Control of flagellar bending: a new agenda based on dynein diversity. *Cell Motil Cytoskeleton* 28(3):199–204.
27. Brokaw CJ, Kamiya R (1987) Bending patterns of Chlamydomonas flagella: IV. Mutants with defects in inner and outer dynein arms indicate differences in dynein arm function. *Cell Motil Cytoskeleton* 8(1):68–75.
28. Mitchell DR, Rosenbaum JL (1985) A motile Chlamydomonas flagellar mutant that lacks outer dynein arms. *J Cell Biol* 100(4):1228–1234.
29. Papon JF, et al. (2010) A 20-year experience of electron microscopy in the diagnosis of primary ciliary dyskinesia. *Eur Respir J* 35(5):1057–1063.
30. Branche C, et al. (2006) Conserved and specific functions of axoneme components in trypanosome motility. *J Cell Sci* 119(Pt 16):3443–3455.
31. Kamiya R, Okamoto M (1985) A mutant of Chlamydomonas reinhardtii that lacks the flagellar outer dynein arm but can swim. *J Cell Sci* 74:181–191.
32. Bui KH, Yagi T, Yamamoto R, Kamiya R, Ishikawa T (2012) Polarity and asymmetry in the arrangement of dynein and related structures in the Chlamydomonas axoneme. *J Cell Biol* 198(5):913–925.
33. Yagi T, Uematsu K, Liu Z, Kamiya R (2009) Identification of dyneins that localize exclusively to the proximal portion of Chlamydomonas flagella. *J Cell Sci* 122(9):1306–1314.
34. Fliegauf M, et al. (2005) Mislocalization of DNAH5 and DNAH9 in respiratory cells from patients with primary ciliary dyskinesia. *Am J Respir Crit Care Med* 171(12):1343–1349.
35. Panizzi JR, et al. (2012) CCDC103 mutations cause primary ciliary dyskinesia by disrupting assembly of ciliary dynein arms. *Nat Genet* 44(6):714–719.
36. Dougherty GW, et al. (2016) DNAH11 Localization in the Proximal Region of Respiratory Cilia Defines Distinct Outer Dynein Arm Complexes. *Am J Respir Cell Mol Biol* 55(2):213–224.
37. Hoops HJ, Witman GB (1983) Outer doublet heterogeneity reveals structural polarity related to beat direction in Chlamydomonas flagella. *J Cell Biol* 97(3):902–908.
38. Dean AB, Mitchell DR (2015) Late steps in cytoplasmic maturation of assembly-competent axonemal outer arm dynein in Chlamydomonas require interaction of ODA5 and ODA10 in a complex. *Mol Biol Cell* 26(20):3596–3605.
39. Wirschell M, et al. (2004) Oda5p, a novel axonemal protein required for assembly of the outer dynein arm and an associated adenylate kinase. *Mol Biol Cell* 15(6):2729–2741.
40. Subota I, et al. (2014) Proteomic analysis of intact flagella of procyclic Trypanosoma brucei cells identifies novel flagellar proteins with unique sub-localisation and dynamics. *Mol Cell Proteomics MCP* 13(7):1769–86.
41. Dean S, Sunter JD, Wheeler RJ (2017) TrypTag.org: A Trypanosome Genome-wide Protein Localisation Resource. *Trends Parasitol* 33(2):80–82.
42. Koutoulis A, et al. (1997) The Chlamydomonas reinhardtii ODA3 gene encodes a protein of the outer dynein arm docking complex. *J Cell Biol* 137(5):1069–1080.
43. Takada S, Wilkerson CG, Wakabayashi K, Kamiya R, Witman GB (2002) The outer dynein arm-docking complex: composition and characterization of a subunit (oda1) necessary for outer arm assembly. *Mol Biol Cell* 13(3):1015–1029.
44. Redmond S, Vadivelu J, Field MC (2003) RNAit: an automated web-based tool for the selection of RNAi targets in Trypanosoma brucei. *Mol Biochem Parasitol* 128(1):115–118.
45. Wheeler RJ, Scheumann N, Wickstead B, Gull K, Vaughan S (2013) Cytokinesis in Trypanosoma brucei differs between bloodstream and tsetse trypomastigote forms: implications for microtubule-based morphogenesis and mutant analysis. *Mol Microbiol* 90(6):1339–55.

46. Gull K, et al. (1990) The cell cycle and cytoskeletal morphogenesis in *Trypanosoma brucei*. *Biochem Soc Trans* 18(5):720–722.
47. Kohl L, Robinson D, Bastin P (2003) Novel roles for the flagellum in cell morphogenesis and cytokinesis of trypanosomes. *EMBO J* 22(20):5336–5346.
48. Sakato M, King SM (2003) Calcium Regulates ATP-sensitive Microtubule Binding by Chlamydomonas Outer Arm Dynein. *J Biol Chem* 278(44):43571–43579.
49. Sakato M, Sakakibara H, King SM (2007) Chlamydomonas Outer Arm Dynein Alters Conformation in Response to Ca²⁺. *Mol Biol Cell* 18(9):3620–3634.
50. Casey DM, Yagi T, Kamiya R, Witman GB (2003) DC3, the Smallest Subunit of the Chlamydomonas Flagellar Outer Dynein Arm-docking Complex, Is a Redox-sensitive Calcium-binding Protein. *J Biol Chem* 278(43):42652–42659.
51. Hoops HJ, Witman GB (1983) Outer doublet heterogeneity reveals structural polarity related to beat direction in Chlamydomonas flagella. *J Cell Biol* 97(3):902–908.
52. Bui KH, Sakakibara H, Movassagh T, Oiwa K, Ishikawa T (2009) Asymmetry of inner dynein arms and inter-doublet links in Chlamydomonas flagella. *J Cell Biol* 186(3):437–446.
53. Hagen KD, et al. (2011) Novel Structural Components of the Ventral Disc and Lateral Crest in Giardia intestinalis. *PLoS Negl Trop Dis* 5(12):e1442.
54. Owa M, et al. (2014) Cooperative binding of the outer arm-docking complex underlies the regular arrangement of outer arm dynein in the axoneme. *Proc Natl Acad Sci* 111(26):9461–9466.
55. Vincensini Laetitia, et al. (2017) Flagellar incorporation of proteins follows at least two different routes in trypanosomes. *Biol Cell* 110(2):33–47.
56. Patel-King RS, King SM (2009) An outer arm dynein light chain acts in a conformational switch for flagellar motility. *J Cell Biol* 186(2):283–295.
57. Lindemann CB, Lesich KA (2010) Flagellar and ciliary beating: the proven and the possible. *J Cell Sci* 123(4):519–528.
58. Lindemann CB (2004) Testing the geometric clutch hypothesis. *Biol Cell* 96(9):681–690.
59. Lindemann CB, Lesich KA (2015) The geometric clutch at 20: stripping gears or gaining traction? *Reproduction* 150(2):R45–R53.
60. Wakabayashi K, King SM (2006) Modulation of Chlamydomonas reinhardtii flagellar motility by redox poise. *J Cell Biol* 173(5):743–754.
61. Hjeij R, et al. (2014) CCDC151 Mutations Cause Primary Ciliary Dyskinesia by Disruption of the Outer Dynein Arm Docking Complex Formation. *Am J Hum Genet* 95(3):257–274.
62. Poon SK, Peacock L, Gibson W, Gull K, Kelly S (2012) A modular and optimized single marker system for generating Trypanosoma brucei cell lines expressing T7 RNA polymerase and the tetracycline repressor. *Open Biol* 2(2):110037.
63. Brun R, Schönenberger M (1979) Cultivation and in vitro cloning or procyclic culture forms of Trypanosoma brucei in a semi-defined medium. Short communication. *Acta Trop* 36(3):289–292.
64. Dean S, et al. (2015) A toolkit enabling efficient, scalable and reproducible gene tagging in trypanosomatids. *Open Biol* 5(1):140197.
65. Inoue M, et al. (2005) The 14-3-3 Proteins of Trypanosoma brucei Function in Motility, Cytokinesis, and Cell Cycle. *J Biol Chem* 280(14):14085–14096.
66. Beneke T, et al. (2017) A CRISPR Cas9 high-throughput genome editing toolkit for kinetoplastids. *Open Sci* 4(5):170095.
67. Dean S, Moreira-Leite F, Varga V, Gull K (2016) Cilium transition zone proteome reveals compartmentalization and differential dynamics of ciliopathy complexes. *Proc Natl Acad Sci* 113(35):E5135–E5143.
68. Collins TJ (2007) ImageJ for microscopy. *BioTechniques* 43(1 Suppl):25–30.
69. Höög JL, Gluenz E, Vaughan S, Gull K (2010) Ultrastructural investigation methods for Trypanosoma brucei. *Methods Cell Biol* 96:175–196.
70. Gluenz E, Wheeler RJ, Hughes L, Vaughan S (2015) Scanning and three-dimensional electron microscopy methods for the study of Trypanosoma brucei and Leishmania mexicana flagella. *Methods Cell Biol* 127:509–542.
71. Gadelha C, Wickstead B, McKean PG, Gull K (2006) Basal body and flagellum mutants reveal a rotational constraint of the central pair microtubules in the axonemes of trypanosomes. *J Cell Sci* 119(Pt 12):2405–2413.
72. Wheeler RJ, Gluenz E, Gull K (2015) Basal body multipotency and axonemal remodelling are two pathways to a 9+0 flagellum. *Nat Commun* 6:8964.

73. Markham R, Frey S, Hills GJ (1963) Methods for the enhancement of image detail and accentuation of structure in electron microscopy. *Virology* 20(1):88–102.
74. Hughes LC, Ralston KS, Hill KL, Zhou ZH (2012) Three-Dimensional Structure of the Trypanosome Flagellum Suggests that the Paraflagellar Rod Functions as a Biomechanical Spring. *PLoS ONE* 7(1):e25700.
75. Moran U, Milo R, Jorgensen PC, Weber GM, Springer M (2009) BioNumbers—The Database of Key Numbers in Molecular and Cell Biology. Available at: <https://dash.harvard.edu/handle/1/8063390> [Accessed October 20, 2017].
76. Mullineaux CW, Nenninger A, Ray N, Robinson C (2006) Diffusion of Green Fluorescent Protein in Three Cell Environments in *Escherichia Coli*. *J Bacteriol* 188(10):3442–3448.
77. Tyler KM, Matthews KR, Gull K (2001) Anisomorphic cell division by African trypanosomes. *Protist* 152(4):367–378.
78. Fort C, Bonnefoy S, Kohl L, Bastin P (2016) Intraflagellar transport is required for the maintenance of the trypanosome flagellum composition but not length. *J Cell Sci:jcs.188227*.
79. Aurrecochea C, et al. (2017) EuPathDB: the eukaryotic pathogen genomics database resource. *Nucleic Acids Res* 45(D1):D581–D591.
80. Emms DM, Kelly S (2015) OrthoFinder: solving fundamental biases in whole genome comparisons dramatically improves orthogroup inference accuracy. *Genome Biol* 16:157.
81. Hodges ME, Wickstead B, Gull K, Langdale JA (2011) Conservation of ciliary proteins in plants with no cilia. *BMC Plant Biol* 11:185.
82. Lupas A, Dyke MV, Stock J (1991) Predicting coiled coils from protein sequences. *Science* 252(5009):1162–1164.
83. Wilson D, et al. (2009) SUPERFAMILY—sophisticated comparative genomics, data mining, visualization and phylogeny. *Nucleic Acids Res* 37(suppl_1):D380–D386.
84. Crooks GE, Hon G, Chandonia J-M, Brenner SE (2004) WebLogo: A Sequence Logo Generator. *Genome Res* 14(6):1188–1190.

Figure Legends

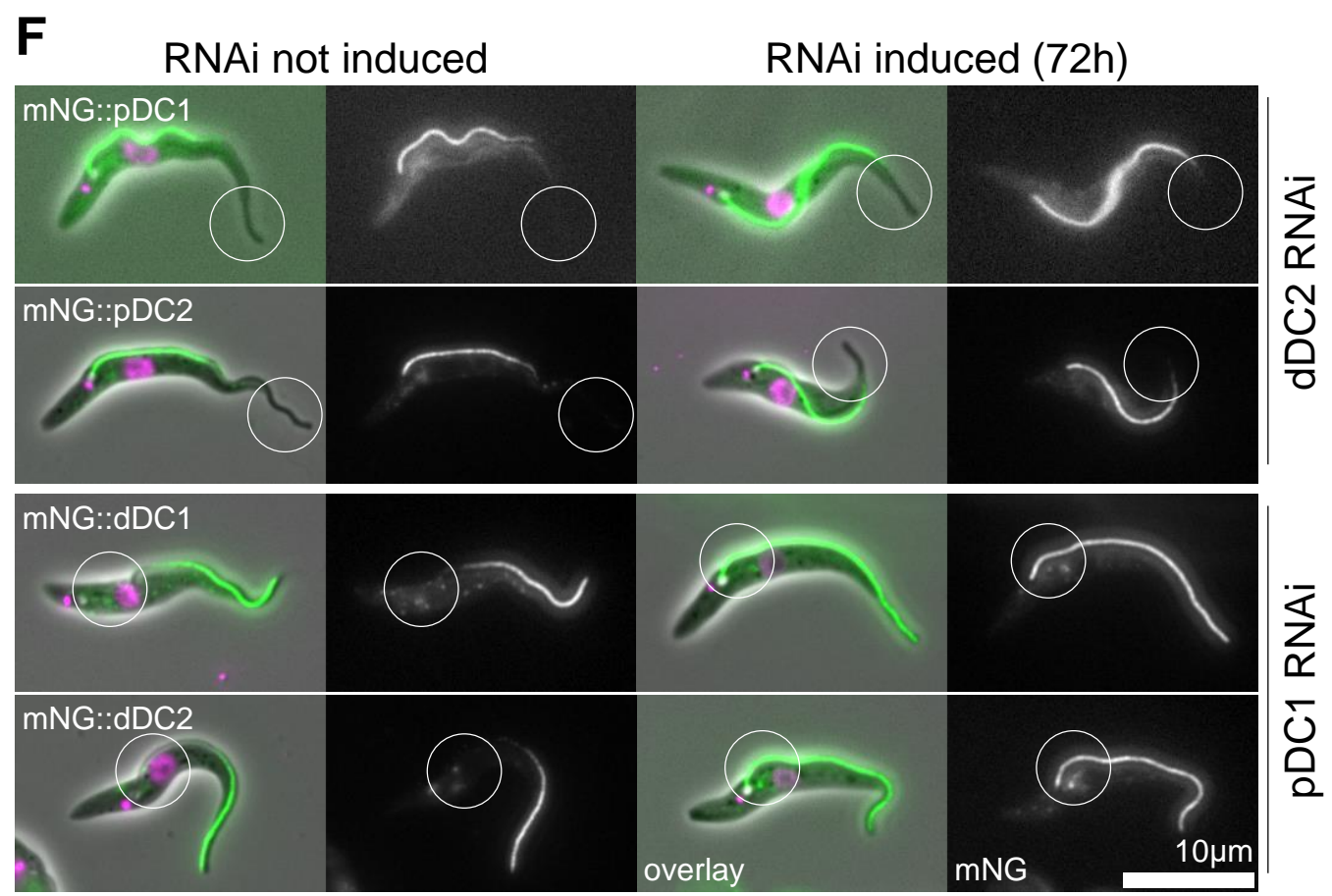
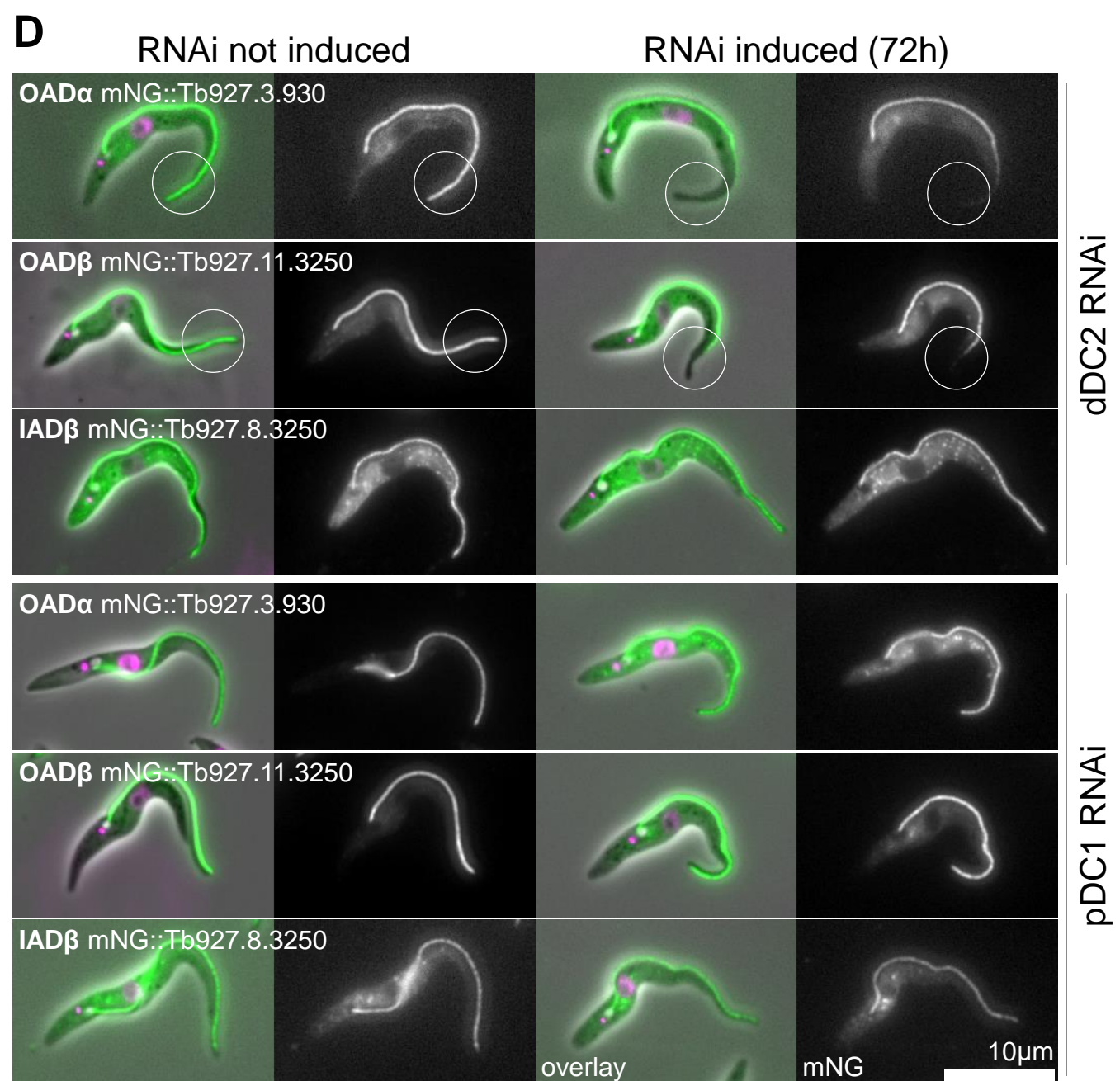
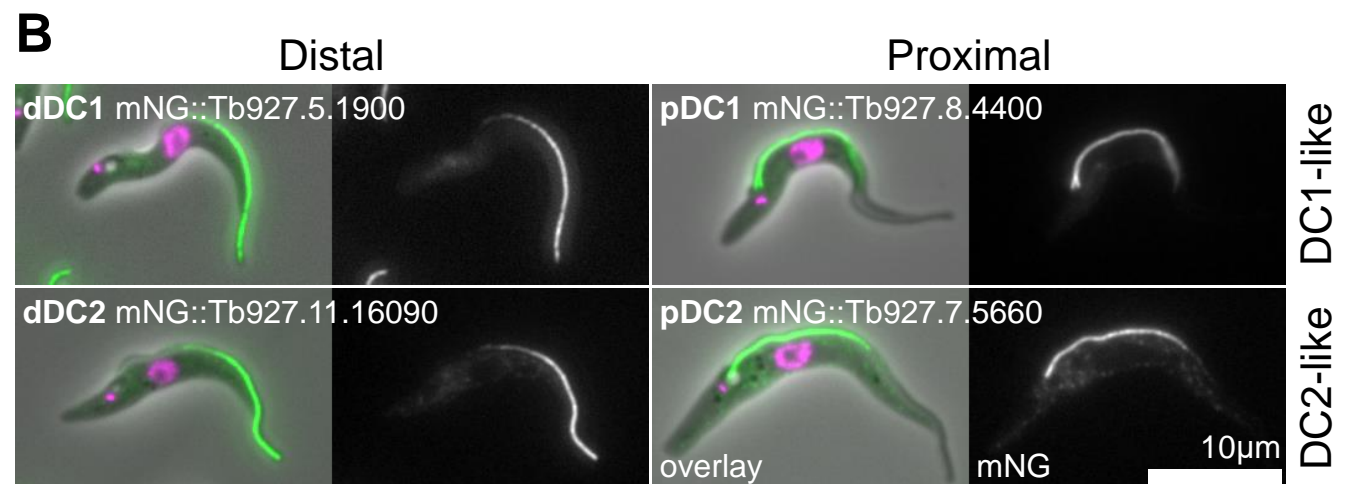
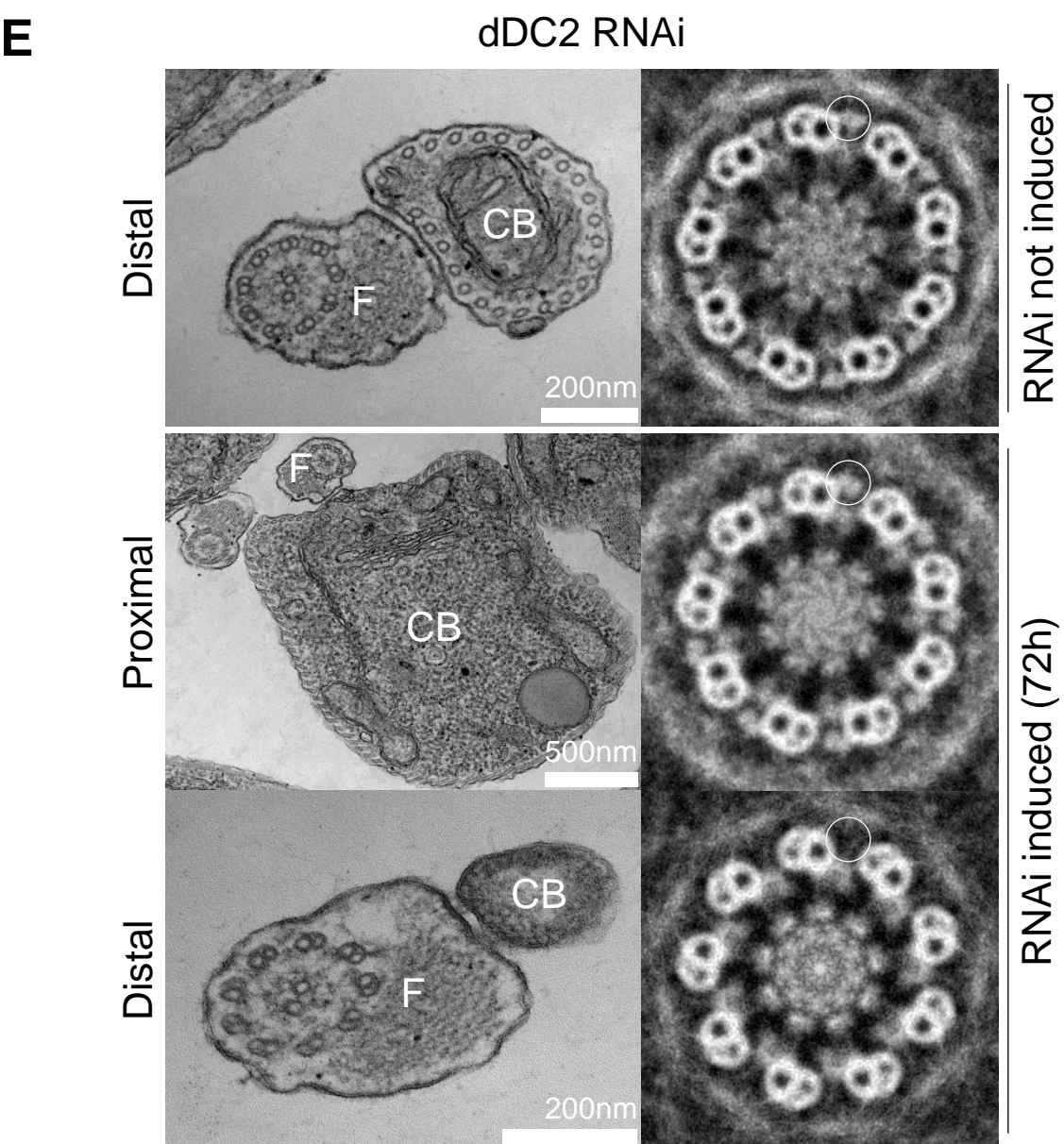
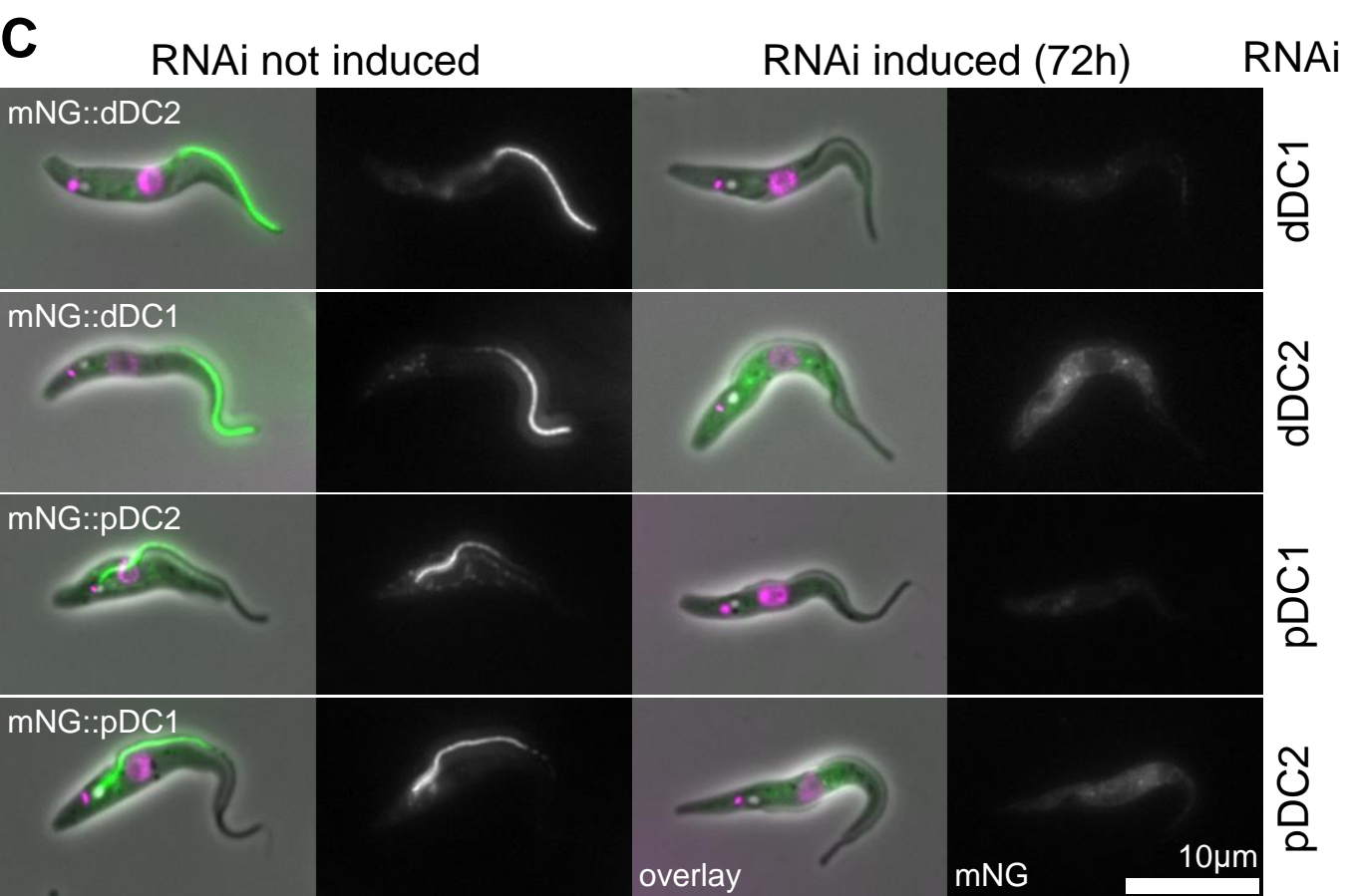
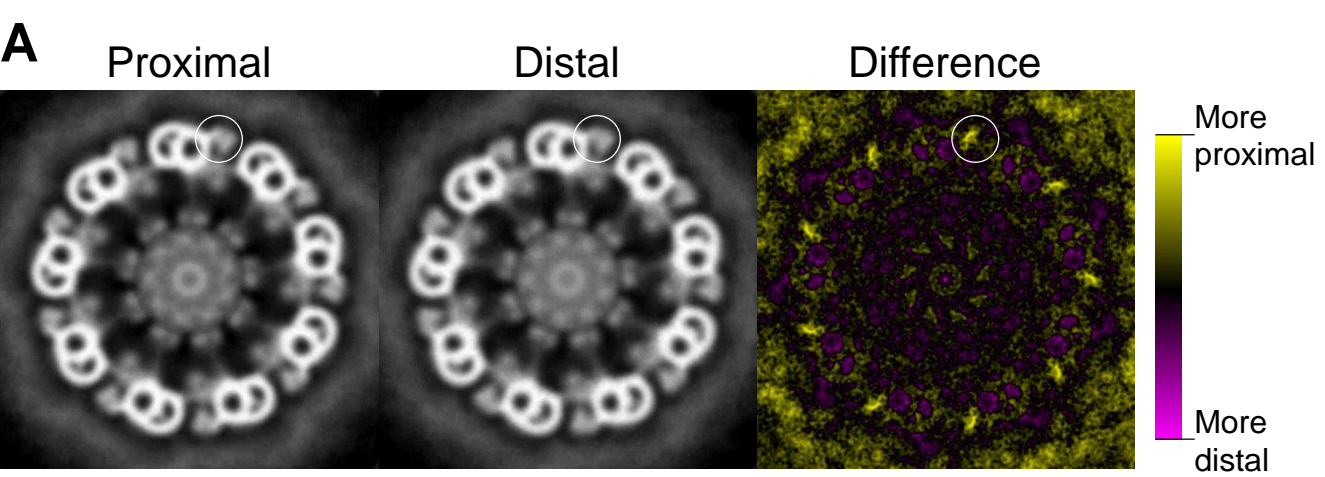
Figure 1. The trypanosome flagellum has proximal/distal asymmetry arising from proximal and distal-specific outer dynein arm DCs. **A.** Nine-fold rotational averages of TEM of transverse sections through the *T. brucei* axoneme. Averages were generated from either the proximal ($n=23$) or distal ($n=24$) region. A difference map shows differences only in the outer dynein arms. **B.** Widefield epifluorescence micrographs of *T. brucei* cells expressing DC proteins tagged with mNG at the N terminus. Overlays of phase contrast (grey), DNA (Hoechst 33342, magenta) and mNG (green) images and mNG fluorescence alone are shown. **C.** Micrographs of *T. brucei* RNAi cells targeting dDC1, dDC2, pDC1 or pDC2 ORFs and respectively expressing mNG tagged dDC2, dDC1, pDC2 or pDC1. Induction of RNAi for 72 h caused loss of fluorescence signal in each case. Summarised in Table 1. **D.** Micrographs of *T. brucei* RNAi cell lines targeting dDC2 or pDC1 expressing mNG tagged OAD α , OAD β or IAD β . Induction of dDC2 RNAi for 72 h caused loss of distal OAD α and OAD β (circled) while pDC1 RNAi had no effect on OAD α and OAD β fluorescence. **E.** TEMs (left) and nine-fold rotational averages (right) of transverse sections through the axoneme of the *T. brucei* dDC2 RNAi cell line. Outer dynein arms are present in uninduced samples (representative of $n=25$) and in the proximal axoneme 72 h after induction of RNAi (representative of $n=11$), but absent in the distal axoneme after 72 h induction of RNAi (representative of $n=7$). CB cell body, F flagellum. **F.** Micrographs of *T. brucei* RNAi cell lines targeting dDC2 or pDC1 and respectively expressing mNG tagged pDC1 or dDC2. 72 h induction of dDC2 RNAi caused distal extension of pDC1 and pDC2 fluorescent signal (circled), and 72 h induction of pDC1 RNAi caused proximal extension of dDC1 and dDC2 fluorescent signal (circled). Summarised in Table 1.

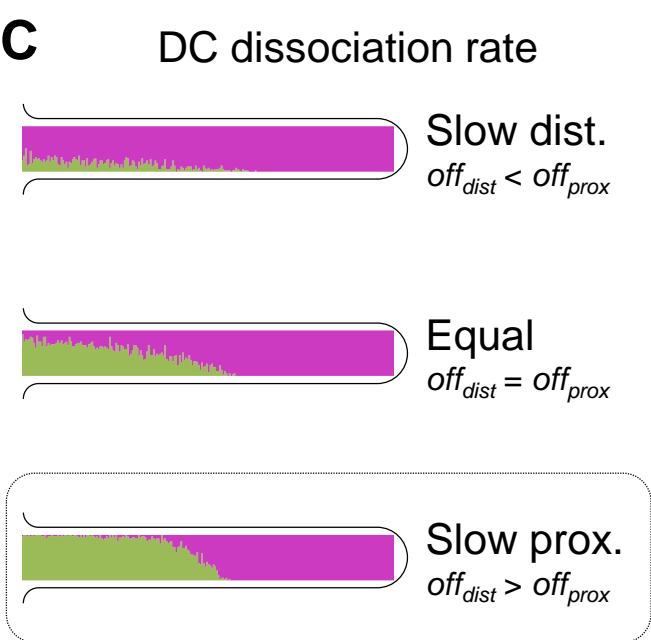
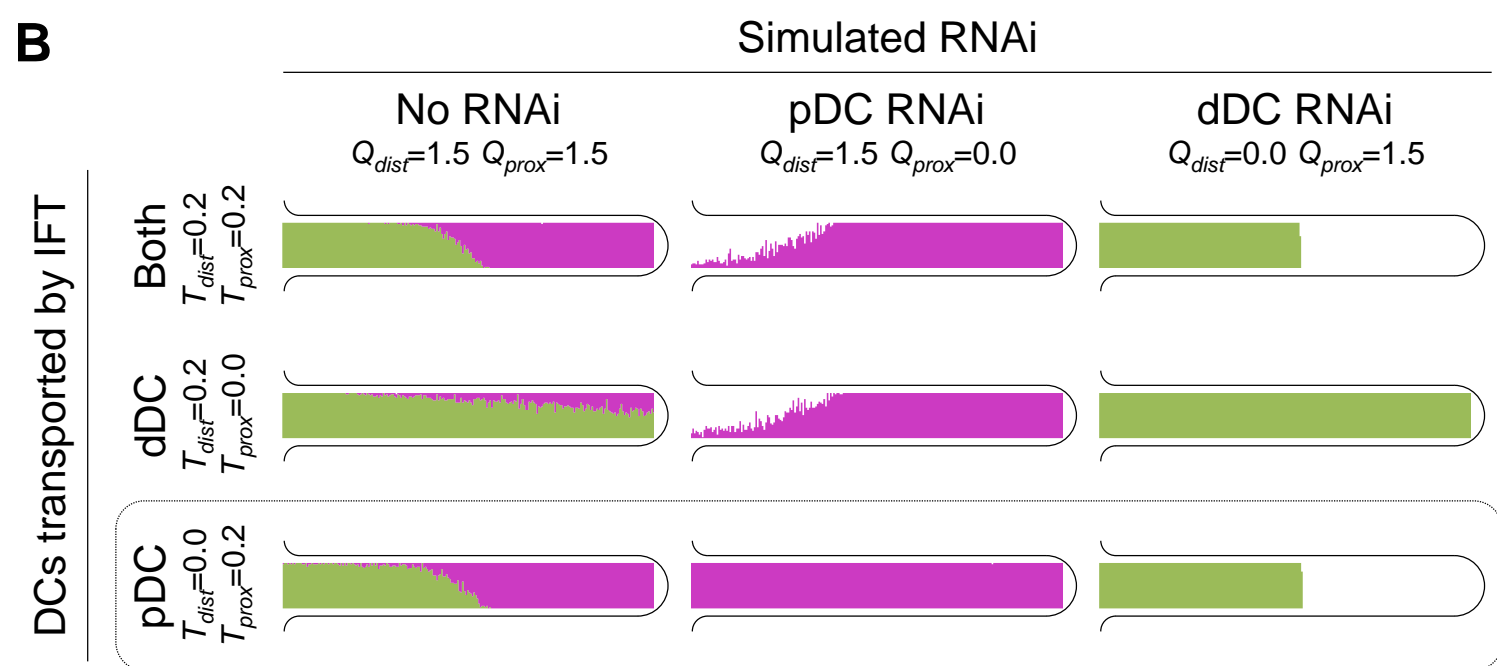
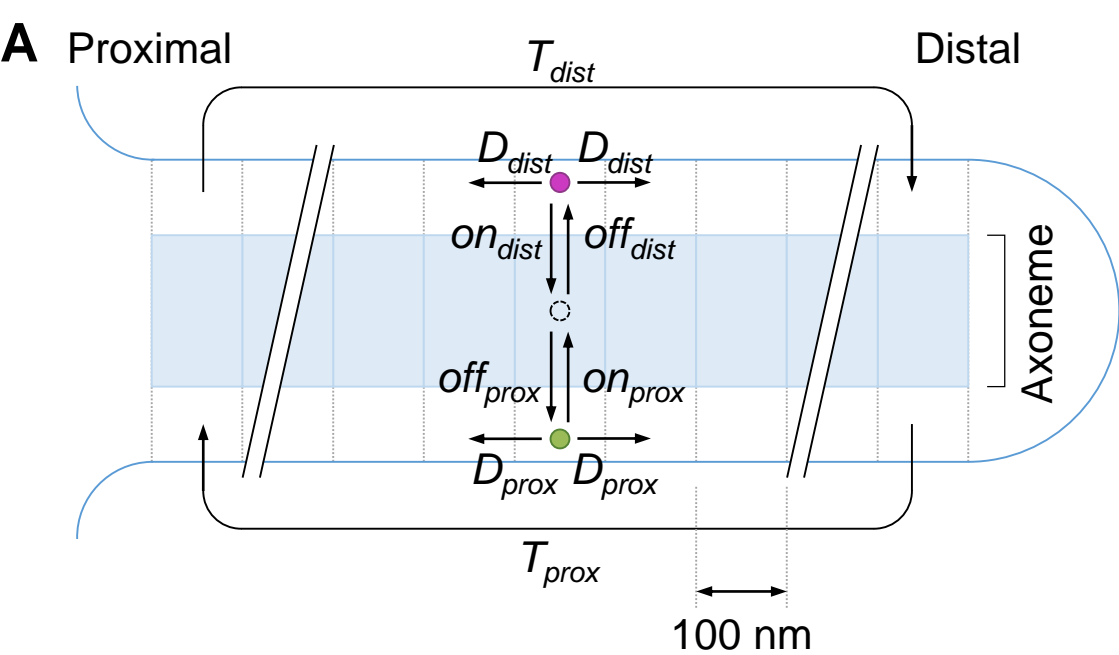
Figure 2. Retrograde movement of proximal DCs by IFT is responsible for proximal/distal axoneme asymmetry. **A.** Outline of the agent based model of DC distribution by IFT and diffusion, showing key parameters: D_{prox} and D_{dist} , the probability of diffusion of proximal or distal DCs to the neighbouring axoneme segment; on_{prox} and on_{dist} , the probability of DC binding; off_{prox} and off_{dist} , the probability of DC unbinding; T_{prox} and T_{dist} , the capacity for anterograde and retrograde IFT transport; and Q_{prox} and Q_{dist} (not shown in diagram), the quantity of DCs. **B.** Simulated distribution of proximal (green) and distal (magenta) DCs in full length flagella with different rates of IFT (T_{prox} and T_{dist}) and quantities of proximal and distal DCs (Q_{prox} and Q_{dist}). The conditions $T_{prox} = 0.2$ and $T_{dist} = 0.0$ (retrograde transport of proximal DCs) of most closely matched the experimental data (Figure 1F). **C.** Simulated distribution of proximal and distal DCs in full length flagella with different rates of dissociation of DCs (off_{prox} and off_{dist}). The condition $off_{prox} < off_{dist}$ most closely matched the experimental data (Figure 1B). **D.** Comparison of simulated distribution of proximal and distal DCs in growing

flagella (left) to micrographs of dividing cells with a new growing flagellum (middle). In the micrographs the new flagellum is indicated (dotted outline) in a *T. brucei* cell line expressing mNG tagged pDC1 and mSc tagged dDC2. Measured proportion of flagellum with dDC2 signal was always approximately 50%, independent of flagellum length (right). **E.** Comparison of simulation of new protein incorporation in a new growing flagellum (left) to micrographs of *T. brucei* cells in an equivalent pulse-chase experiment (right). In the micrographs the new growing flagellum is indicated (dotted outline) in a *T. brucei* cell line expressing HaloTag tagged dDC2 or pDC1 labelled with a 45 min pulse of tetramethylrhodamine HaloTag ligand. The flagellum was labelled with an anti-PFR antibody. **F.** Comparison of simulated distribution of proximal and distal DCs in growing flagella with or without IFT transport of the distal DC and with no IFT transport and reduced quantity of distal DC (left), in comparison to micrographs of dividing cells in a *T. brucei* cell line expressing N terminally mNG tagged pDC1 and N terminally mSc tagged dDC2 8 h after induction of IFT46 RNAi knockdown (right). In the simulation and the new flagellum of dividing cells reduced IFT caused a shorter region of distal DC/dDC2 signal.

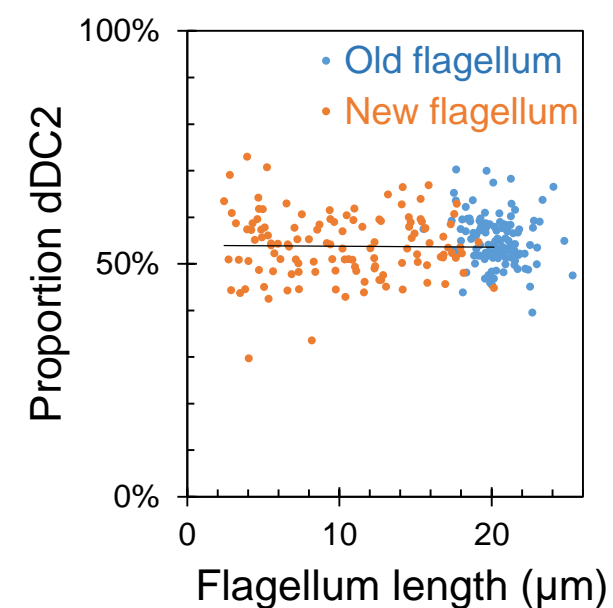
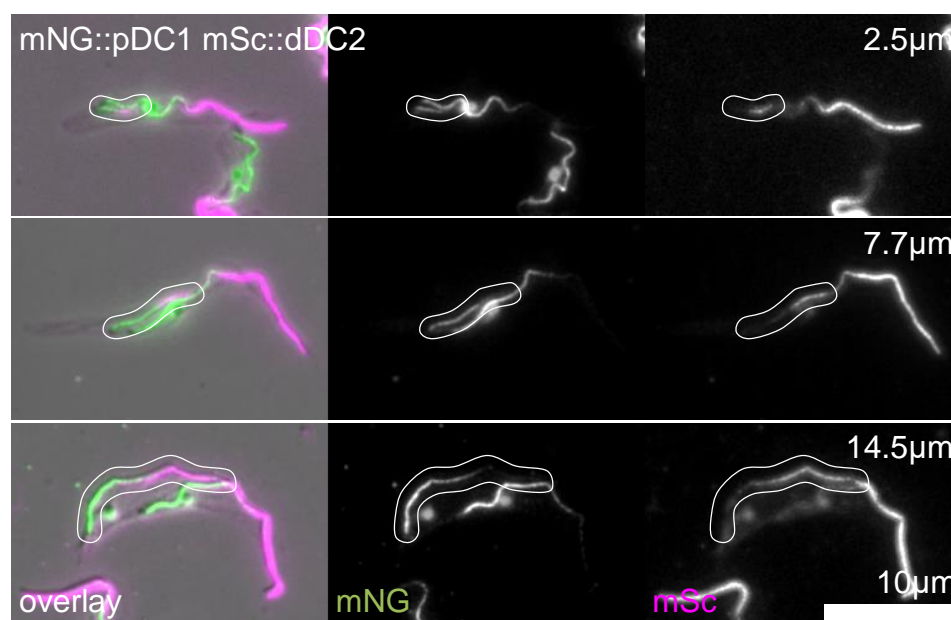
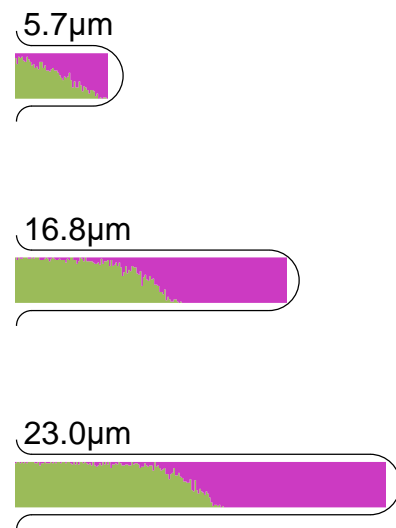
Figure 3. A calcium-binding LC4-like protein is a candidate regulator of the flagellar beat. **A.** Sequence logo of the Ca^{2+} binding site of 100 reference EF-hand domains, and the aligned *T. brucei* and *L. mexicana* LC4-like sequences. **B.** Micrographs of a *T. brucei* cell line with integrated RNAi constructs targeting dDC2 or pDC1 and expressing LC4-like tagged with mNG at the N terminus. 72 h induction of dDC2 RNAi causes loss of flagellar LC4-like signal, and 72 h induction of pDC1 RNAi causes proximal extension of LC4-like signal (circled). Summarised in Table 1. **C.** Micrographs of a *T. brucei* cell line with an integrated RNAi construct targeting LC4-like and expressing dDC2 or pDC1 tagged with mNG at the N terminus. 72 h induction of LC4-like RNAi causes no change in pDC1 or dDC2 signal. Summarised in Table 1.

Figure 4. Proximal/distal flagellum asymmetry contributes to control of flagellum beat type. **A.** Swimming paths, swimming speed and directionality of *L. mexicana* cell lines with deletion of both alleles of dDC2 or LC4-like in comparison to the parental cell line. Swimming tracks show slower, less directional, swimming following dDC2 deletion, which occasionally corresponds to tight helical paths (circled). dDC2 deletion caused a significant decrease in speed, velocity and proportion of highly directional (>0.5) cells, while LC4-like deletion caused a significant increase in speed and velocity (Student's T-test). **B.** Proportion of cells undergoing different types of flagellar movement for *L. mexicana* cell lines with deletion of both alleles of dDC2 or LC4-like in comparison to the parental cell line. Behaviours were assessed from a 4 s 200 Hz videomicrograph. dDC2 deletion caused significantly more ciliary and uncoordinated movement, and LC4-like caused significantly more uninterrupted flagellar type movement (χ^2 test, $p < 10^{-9}$). **C.** Example kymographs of flagellar movement illustrating the types of flagellar movement used as classes in **B.** **D.** Frames from high speed videos corresponding to the kymographs in **C.** Propagation of a flagellum wave over the frames is indicated (white arrow) relative to the cell posterior (black arrow).

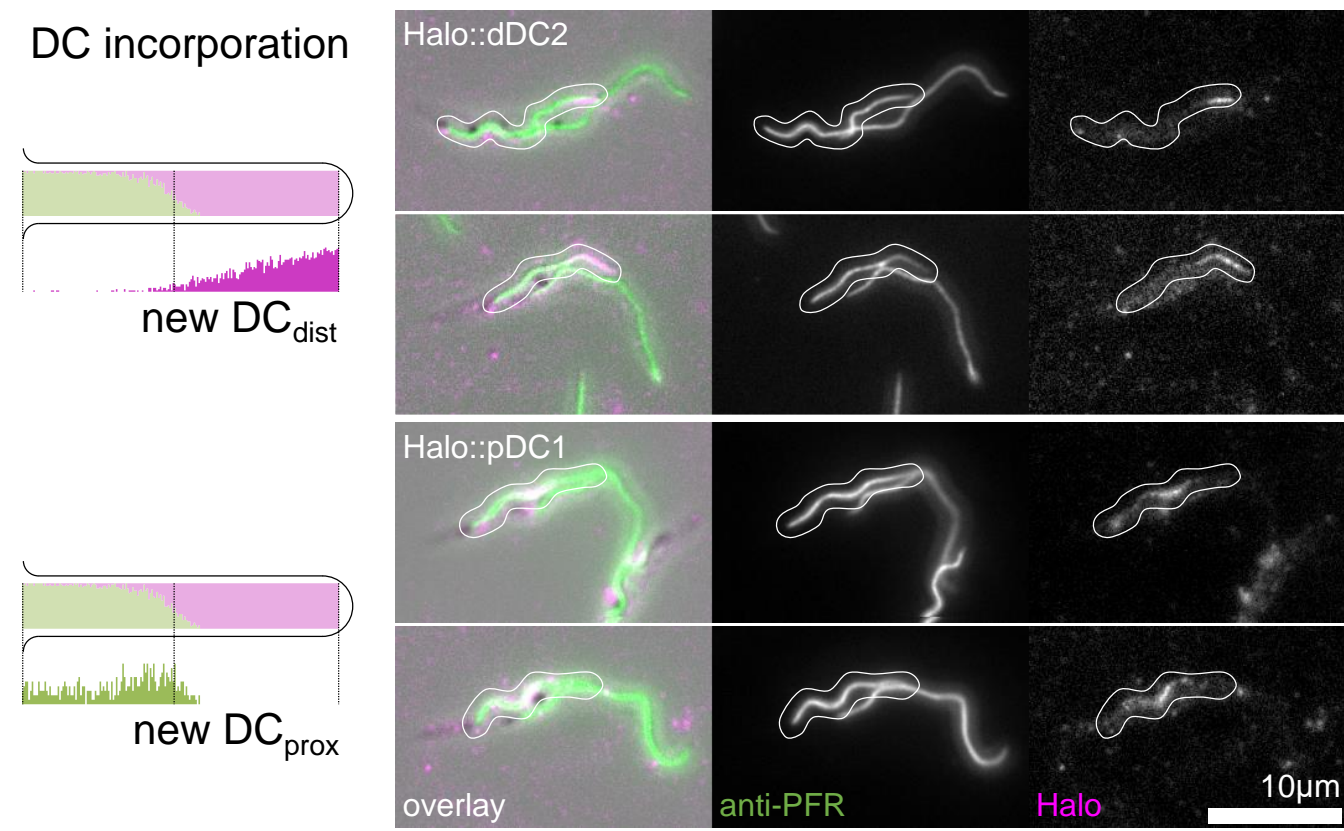




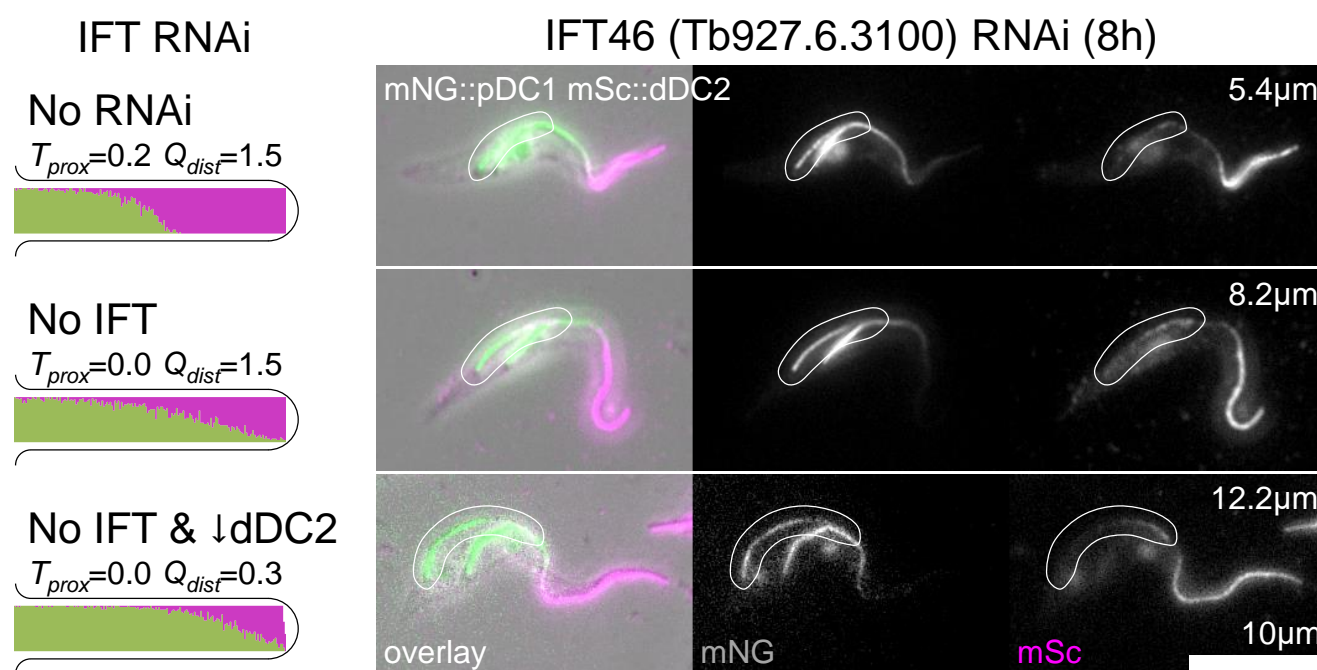
D Flagellum growth

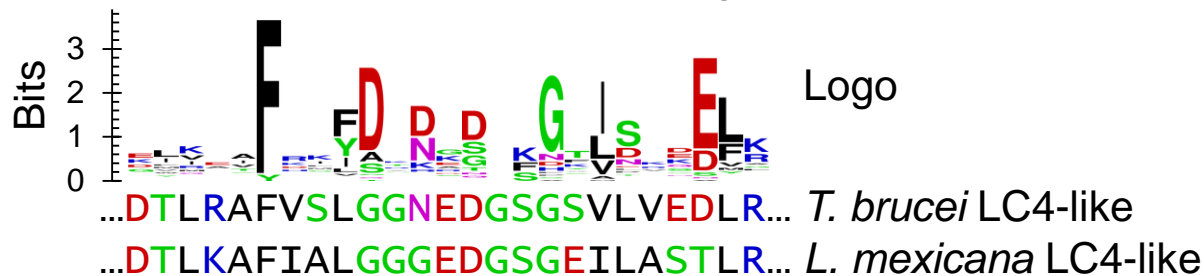


E DC incorporation



F



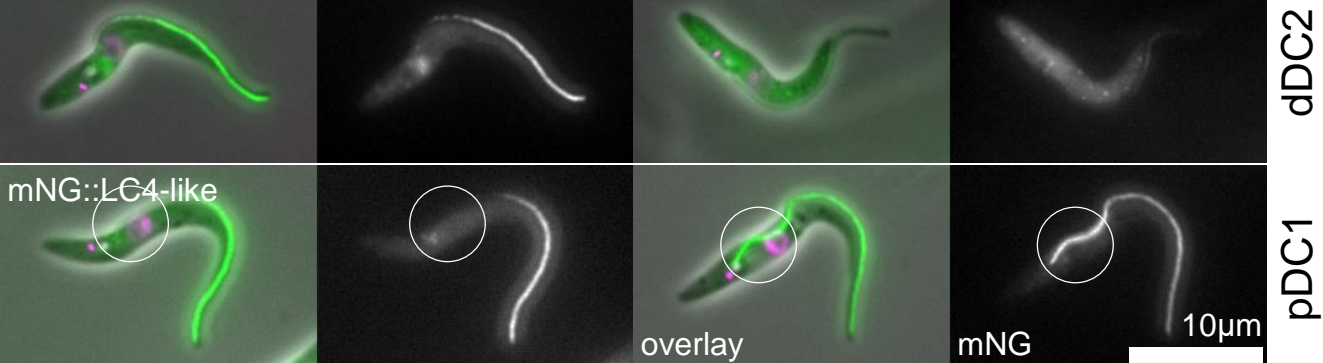
AEF-hand (SSF47473) Ca²⁺ binding site**B**

RNAi not induced

RNAi induced (72h)

RNAi

LC4-like mNG::Tb927.9.4420

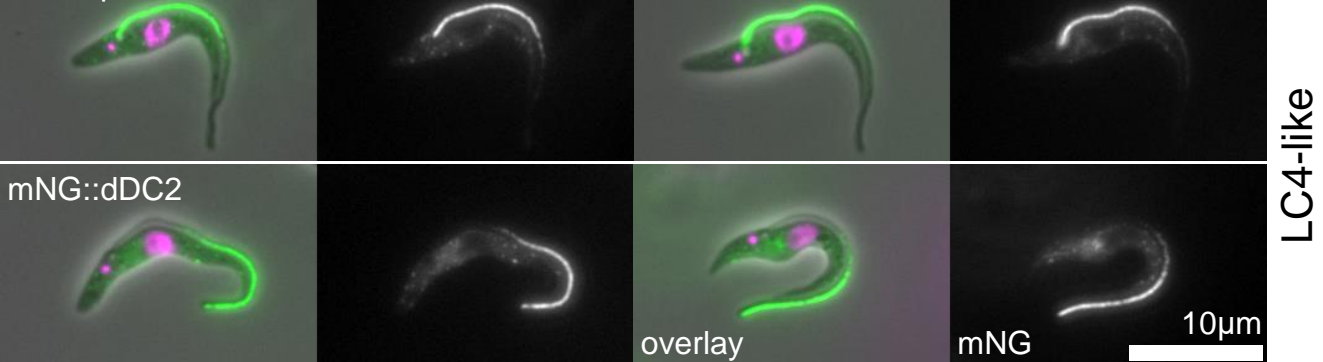
**C**

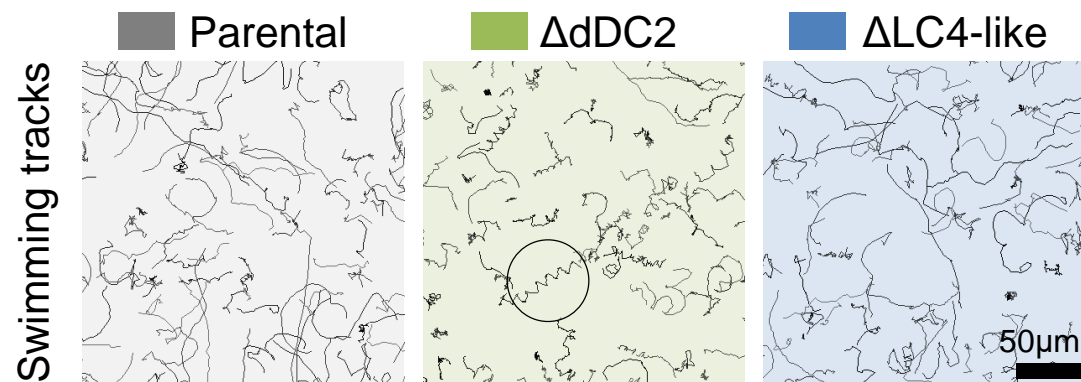
RNAi not induced

RNAi induced (72h)

RNAi

mNG::pDC1



A

μ m/s

Velocity

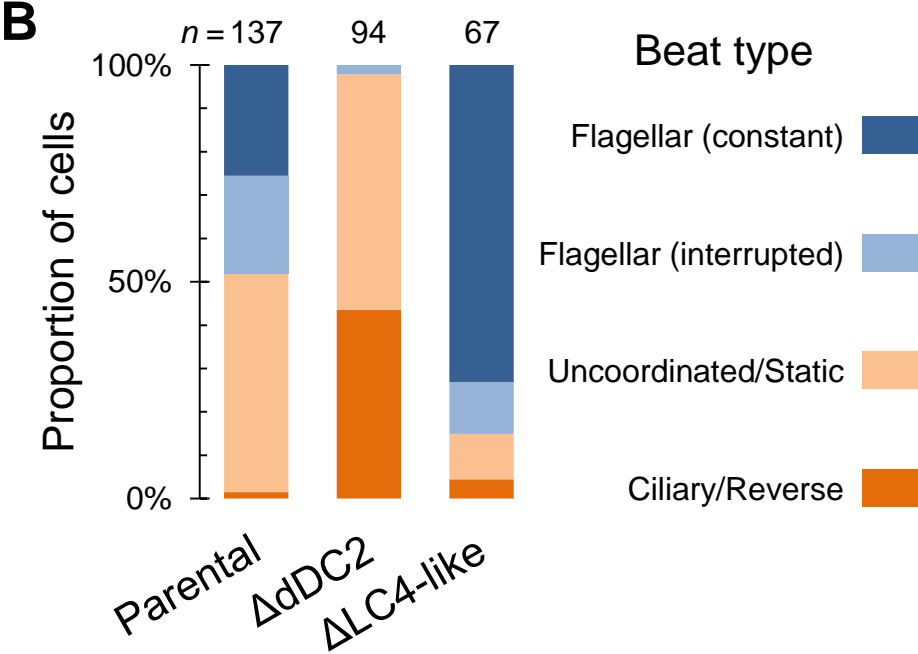
Speed

Proportion

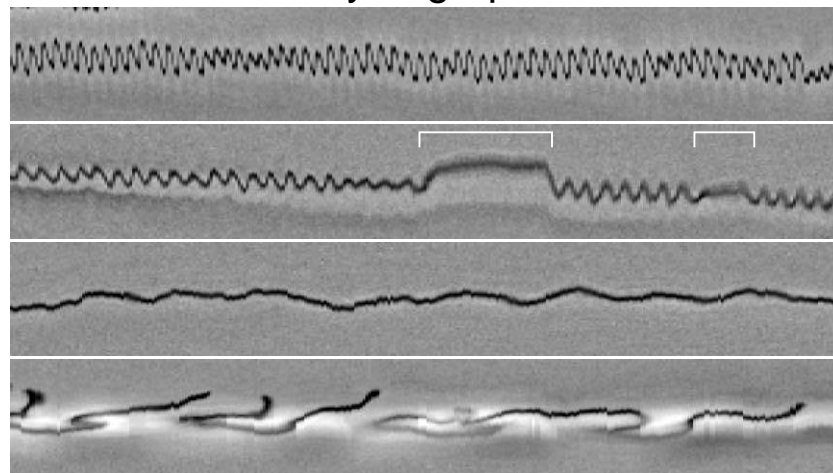
>0.5

<0.5

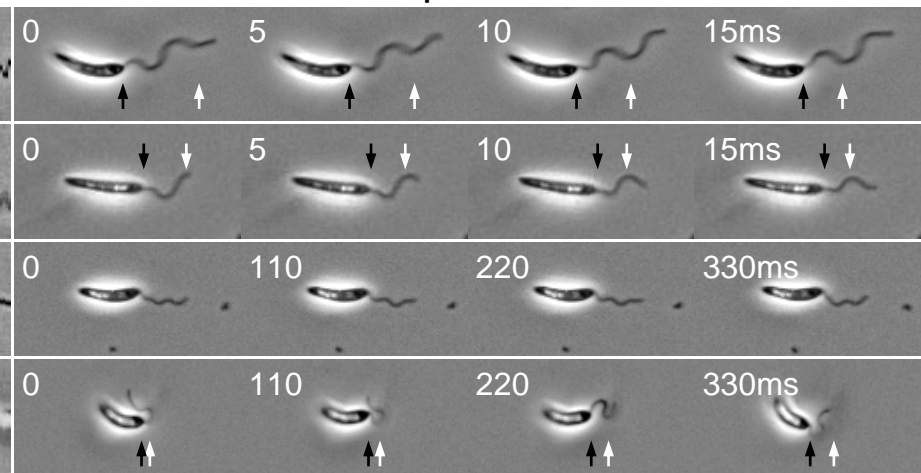
Directionality

B**C**

Kymograph

**D**

Example frames



		No RNAi	dDC1	dDC2	pDC1	pDC2
Protein tagged	dDC1	Distal 50%	0% (No signal)	0% (No signal)	100% (Whole flagellum)	100% (Whole flagellum)
	dDC2	Distal 50%	0% (No signal)	0% (No signal)	100% (Whole flagellum)	100% (Whole flagellum)
	pDC1	Proximal 50%	Proximal 75%	Proximal 75%	0% (No signal)	0% (No signal)
	pDC2	Proximal 50%	Proximal 75%	Proximal 75%	0% (No signal)	0% (No signal)

Table 1. Summary of DC protein localisation changes upon DC RNAi knockdowns in *T. brucei*.

		No RNAi	dDC2	pDC1	LC4-like
Protein tagged	dDC2	Distal 50%	0% (No signal)	100% (Whole flagellum)	Distal 50%
	pDC1	Proximal 50%	Proximal 75%	0% (No signal)	Proximal 50%
	LC4-like	Distal 50%	0% (No signal)	100% (Whole flagellum)	0% (No signal)

Table 2. Summary of evidence for LC4-like localisation dependent on distal DCs in *T. brucei*.



Supplementary Information for

Direction of flagellum beat propagation is controlled by proximal/distal
outer dynein arm asymmetry

Beatrice FL Edwards*, Richard J Wheeler*, Amy R Barker*, Flávia F Moreira-Leite,
Keith Gull, Jack D Sunter

* Equal contribution

Corresponding authors: Richard J Wheeler, Jack D Sunter

Email: richard.wheeler@path.ox.ac.uk, jsunter@brookes.ac.uk

This PDF file includes:

Figure S1 to S3
Table S1
Captions for movie S1

Other supplementary materials for this manuscript include the following:

Movies S1

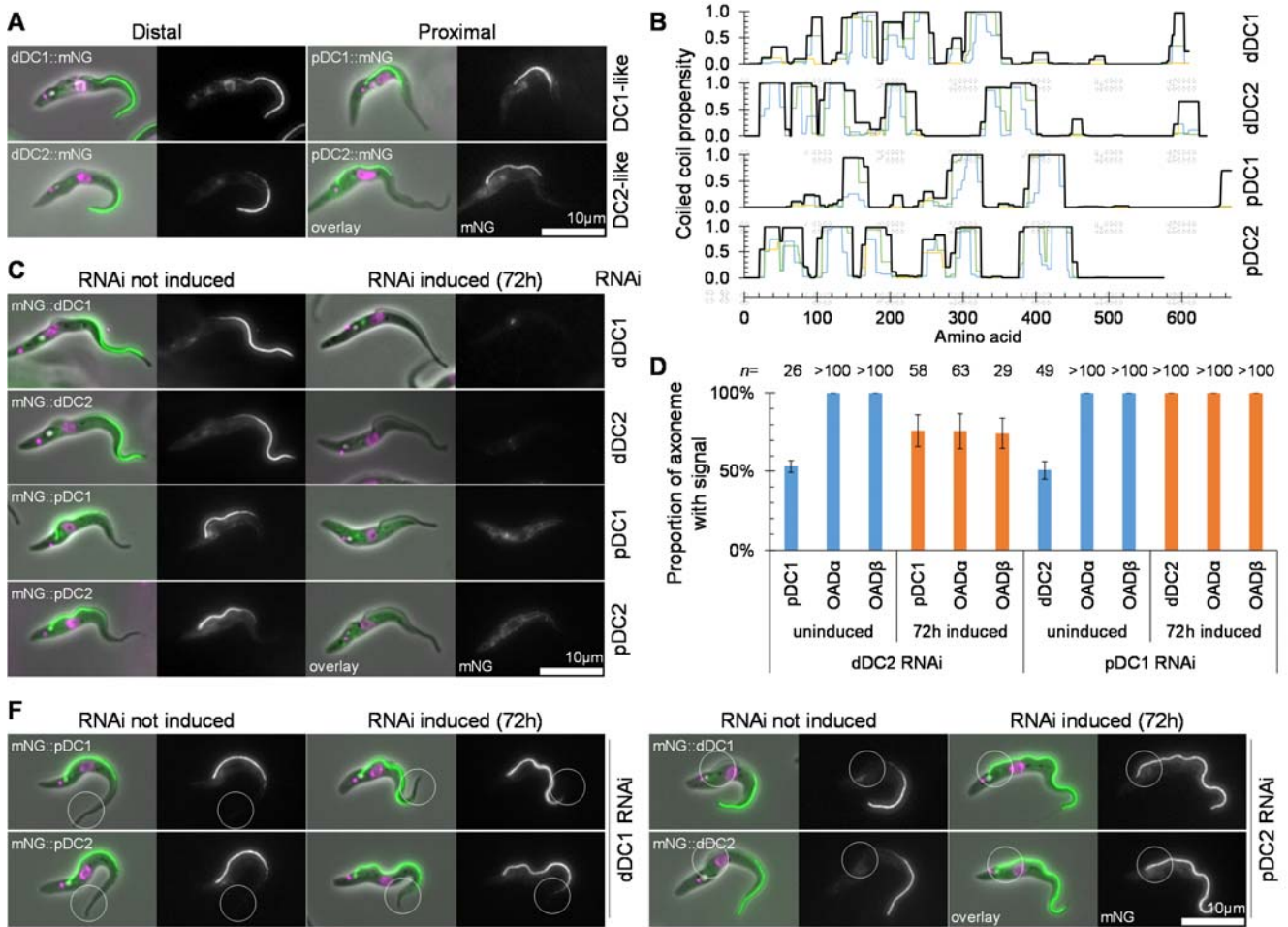


Figure S1 (related to Figure 1). DC proximal/distal asymmetry is present irrespective of the terminus tagged, and RNAi constructs are effective at knocking down tagged DC protein. A. Widefield epifluorescence micrographs of mNG native fluorescence in *T. brucei* cells expressing DC proteins tagged with mNG at the C terminus. Phase contrast (grey), DNA (Hoechst 33342, magenta) and mNG (green) overlay and mNG fluorescence are shown. Localisations are the same as with N terminal tagging (Figure 1B). **B.** Predicted coiled coils in *T. brucei* DCs. COILS v2.2 coiled coil propensity with a window of 14 (blue), 21 (green) and 28 (yellow) and the maximum of all three (black). **C.** Micrographs of *T. brucei* cell lines with integrated inducible RNAi constructs targeting dDC1, dDC2, pDC1 or pDC2 protein open reading frame and expressing the same proteins tagged with mNG at the N terminus. 72 h induction of RNAi causes loss of flagellar mNG signal showing effective knockdown of the mNG DC fusion protein. **D.** Proportion of the axoneme with fluorescent signal from pDC1, OADα or OADβ tagged with mNG at the N terminus before and 72 h after induction of dDC2 RNAi, and dDC2, OADα or OADβ tagged with mNG at the N terminus before and 72 h after induction of pDC1 RNAi. This is a quantitation of the phenomenon illustrated in Figure 1D,F. For samples with 100% axoneme signal all examples of >100 cells had no region lacking signal. Error bars indicate standard deviation. **E.** Micrographs of *T. brucei* RNAi cell lines targeting dDC1 or pDC2 and respectively expressing mNG tagged pDC1 or dDC2. 72 h induction of dDC1 RNAi caused distal extension of pDC1 and pDC2 fluorescent signal (circled), and 72 h induction of pDC2 RNAi caused proximal extension of dDC1 and dDC2 fluorescent signal (circled). Summarised in Table 1.

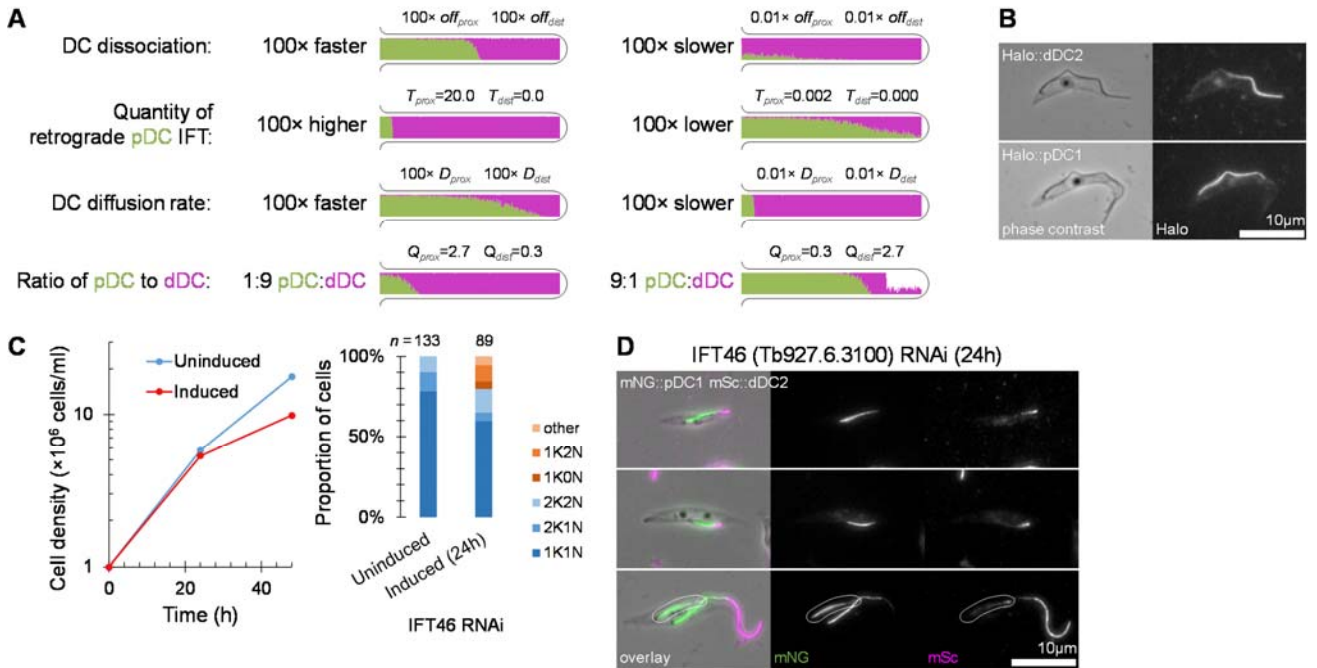


Figure S2 (related to Figure 2). Controls for analysing the mechanism of axoneme proximal/distal docking complex asymmetry. **A.** Behaviour of the agent-based model of proximal/distal axoneme asymmetry with large changes to parameters: 100-fold larger or smaller values of off , T or D and unequal values of Q_{prox} and Q_{dist} . Large parameter changes still give proximal distal/asymmetry, although the quantitative features are altered. **B.** Micrographs of *T. brucei* cell lines expressing N terminally HaloTag tagged dDC2 or pDC1 following 45 min incubation with tetramethylrhodamine HaloTag ligand (no blocking step) to label all DC protein. HaloTag tagged dDC2 and pDC1 have the same localisation as mNG tagged dDC2/pDC1, cf. Figure 1B, S1B. **C.** Summary of the phenotype caused by IFT46 RNAi knockdown. Following RNAi induction, population growth is slowed and the proportion of cells with normal numbers of nuclei (N) and kinetoplasts (K) (1K1N, 2K1N, 2K2N; blue shades) are reduced, and 1K2N and 1K0N cells (indicating cytokinesis defects; orange shades) are more prevalent. **D.** Micrographs of *T. brucei* cells expressing N terminally mNG tagged pDC1 and N terminally mSc tagged dDC2 (as in Figure 2F) 24 h after induction of IFT46 RNAi knockdown. After a longer IFT46 RNAi induction many flagella are abnormally short, both on cells with one flagellum and the new flagellum of dividing cells. Abnormally short flagella have a very short region of dDC2 signal.

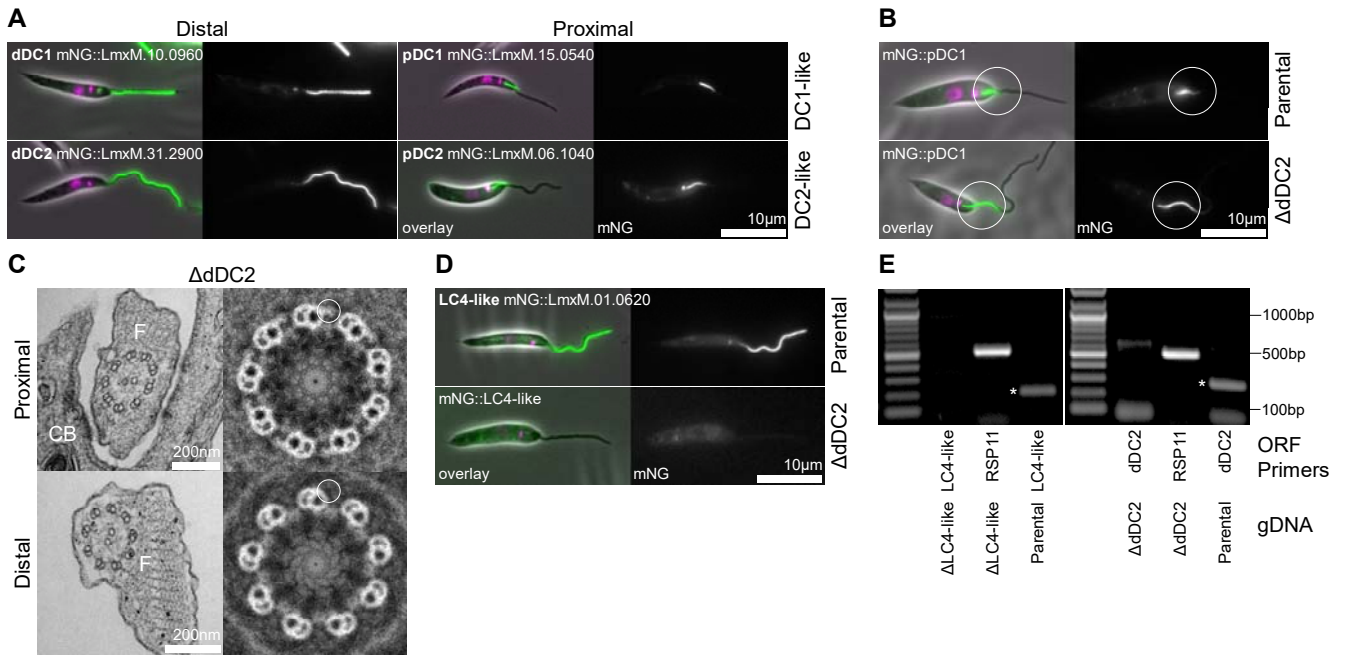


Figure S3 (related to Figure 4). *L. mexicana* has similar proximal/distal axoneme asymmetry to *T. brucei*. **A.** Widefield epifluorescence micrographs of mNG native fluorescence in *L. mexicana* cells expressing DC proteins tagged with mNG at the N terminus, cf. Figure 1B. Phase contrast (grey), DNA (Hoechst 33342, magenta) and mNG (green) overlay and mNG fluorescence are shown. **B.** Micrographs of *L. mexicana* cell lines expressing pDC1 tagged with mNG at the N terminus, before and after deletion of both alleles of dDC2. dDC2 deletion causes distal extension of pDC1 fluorescent signal (circled), cf. Figure 1F. **C.** Transmission electron micrographs (left) and nine-fold rotational averages (right) of transverse sections through the axoneme of the *L. mexicana* dDC2 deletion cell line. Outer dynein arms are present in the proximal axoneme (representative of $n=8$), but absent in the distal axoneme (representative of $n=9$). CB cell body, F flagellum. **D.** Micrographs of *L. mexicana* cell lines expressing LC4-like tagged with mNG at the N terminus showing a distal axoneme localisation, cf. Figure 3C. **E.** PCR confirmation of deletion both alleles of LC4-like or dDC2 open reading frames in the *L. mexicana* deletion cell lines used for swimming analysis (Figure 3). The asterisk indicates the expected PCR product size when the open reading frame is present.

Table S1. RNAi target sequences.

Gene	Primers	RNAi target sequence
Tb927.8.4400	ATAATACCAATGTGATGGAT GTCCAAGTCTAGTCGTAAA TATATACCATAGAGTTGGCC CATCCAAGCCTCCAGAGGT	GTCCAAGTCTAGTCGTAAAAATCACTTGCCTATTGCCCTCCGCTTCCAACCAAAGTGCGGATAAGAGGGGAGAGCTGCAGT TGAAGAAGCAAGGACCAGGGGAGCAACCGGCCAATGAGGCTATAACGGTGCCAGATCTGAAACTAGACGAAACAGTCCGC ATAAGGGAAATGTTTACGGAGTATATTAATGGTGAGTATGTAACCACTATTTGACCTTCGCGTGCTCCCTTCAGAGCT TGGAGTATATCCCTCCGACGATGAAATGACACTTGTATGACCGCATTTGAGAACAAAGTGAGTTTTACTAATCTCTGTGA GGTACATGCGGTTTTACAAGAAAGAAATTTTGGAAATCGAACAGCAACGTCACCGTTCCAATGCCGCGCAAGATGAATGC GAGGACACGCTTCGTGCCTTTGTTTCACTTGGTGGAACGAAGATGGAAGTGGGAGCGTCTTAGTGGAGGACTTACGGCA GGTGTGCAGAAACTTCGGCCTCACTATTGATATAAACGAGGCACCTCAATGGTTTGAATGAGTCAGAGAGCCCCCTTAACGT TGCCTATATGGAATTTTGAACCTGTGGAAACATCAAAGCCGTGAGCGAGGTGGGAATCGGGAACAATACGCAGCCTT TCCTTAACCGATACCTGTATACCTCTGGAGGCTTGGATGGG
Tb927.7.5660	ATACCAATGTGATGGCGCAT GTAGAGACCGAGTCA ATACCATAGAGTTGGAGCCT TCCTTCGTGAGAAC	CGCATGTAGAGACCGAGTCAGATCGCCTCTCCACTCTGATTGAAGAGGGGAAGGCGATGCGATTGGAATTGACTTGCAA ATCACCATGCAGAACCAGTAGATGCTCTGAGACAGGATCGTGAAGGGGAGATGGTGGAGATTATGAAAGAAACCTCCTT TCTTATTGAAGTGTGCAACCTGCTTGTGTAGGAACGCAGTGAGTGCAGCATCAGCTGGCAGAATTACGAAAGGCGCGAG AGGCAGACGCCGAAGCGTATGAAAAAGCCTTTTACGAGCTTGTGCGGTAGAGGACCGCTAATAAATCCAGGCGCAGAA GTAAGGGAGGGCATTTGACAAGCTGACAGTGAATTAGCTGAAGTTGTCAAGGAGCGCACCGCCGCGGAGCACGATCTTGT AAACAAGCACAAACGAGACCGGTGCTGCTGCCAGGATGATATGGATGAAGACGGTGTAGTGTCTCGAGAGTCAGCTAAAAG AGTTTGAAGTCTACCTCAACCGTCTAGGGAAAATTGTGCGCACTTGCGATCTTGTCTGAGGTGAGAGTTACGTCTGCGAT GAAATGGGGAGCGGTTCCAGTTGTATAATGTATACAAAGCAAAACGAGCGCGCGGGAATTGAGGAGGAGAGAAA TGAGCTAATGAAGAACTCAATACTCTTGTGTACGGTACTGAAAAGCAGCGTCAGGAGCGCGAGGAGGTGAAAAGGTTGC AAAGTCATCTGAAGGACCTGCAAGAGAAACTGAGGCAATCGAAAAGCGGTGAGAGAAGACACGAGCAGTCTAGCTGAA TCAGTTCTTACCTGCAGAAAACATACACTTCTATTGGTTGTGTTGCGCGCAAGCTTGTCTCAGAAAGGAAGGCT
Tb927.5.1900	ATAATACCAATGTGATGGAT GCGTTATCGATGTGGGGCAA TATATACCATAGAGTTGGGC TGCTGCTGTTGCTCTACAT	GCCTCCGAGCCAGCTGTTAAAGACATGGATGAGCGCCGTTGCTGATGGCAGTAACATTGTTGCTGCCAGGATGAAA TTATGCGTCAGCAAGAGGCGGTGCAGAAACTGACTAGCGAGAATGAAAGGTTGAAGAAGGAAATAGCTGTTGCTCCGGG GAGCAGTATGATTATGTTAAAGCGGATAAATATGCAGCCCTAAAACTGAGGTGGACTCACTGGAGCAGCGGTATCAATT TGAAAAGATGCATTTGAACGAGCTTACCAAGCAGTATCAGCTAGCTCGCATTGACCTTATGCAAGGTTTCCAAGCTAAAGG GGGTGTGAACGCAGAGCAAGAAATGTTGAGCGGTACAACGCCAGCTGGAGATACTAGAAAACCCCTAGATCAAGCG CTCGCAGGTTTAAACGACGCTGTTTCTATAACAAAGAGCTGCGCGATCAGATCGATATAATTTCGCGGGGAACGCGCGGT TTTTCAACGTGTACACAAGAAGATGGAGGACGATCTGAGATCTAAGAAAAAATCATGTGCGGAACGGATTGAACAGTCAA ACCAGACCTGGATGAACGAGACGGCTACCTGCAGCAGGTGGAGCAGCTTAGAACAGCGCTTAGCGAGCAGAAGGAGGAA TATGACACCGCTGTGCGTAACCTTGGATGTATGCATGATCGACATCAA
Tb927.11.160 90	ATAATACCAATGTGATGGAT GCCTCCGAGCCAGCTGTTA TATATACCATAGAGTTGGTT GATGTCGATCATGCATACA	GCGTTATCGATGTGGGGCAACGAACAGTGGAGCTCCTGCAGGCAGAAAGTGCGGCACAACAAAGAAATGTCTCACAGCT TTGCGCCTGGAAAAATAACGACTTAATGTAATTCTTCAGCAGGCGCAGCGGGGTGAGCGACGCGGTGTAGAGATCGATCC GCTGCGCGGTGAGGAGGAGCAACTGCATAACAACTTTGCTTGTCTGAAAGCGCAGCCTCAACAGTGTGCACGGAAGAAAG AGGAGCTCACCAAAGAGATTGCGCGGACTGTAGAGGAGACGGGATATATTCTCCAGGAGGGAAAGTTTCAACCGGACAAC TCCGCCATGGGCCAAAAGATTTCGTGGCCTTGAGAACCGTTTGACAAGTGCCCTCATTAAAGCACAAACGAGGTGAATGCCAT TCGCGGCACATACGAGGCGCTTTTGGAGCGGTTACAGCAAGAGCAGGCGGGATTGATACTCAGCTCGCAGCAATGGA AAACGTTGCAGAACAAAGAGAAGGATCTCTGCGATCTCAACACAGTAGCAGCCGAGGCATCGAACGGAAGGGATGCGGCT AAGGCAGAGGTGCTGCGGCTGAAGGCACAACCTTACGCGGAGCGCGGGGCACAAAATAAGGATCTGGAGGAGAGGCGGGC ATTTGTGATGACGAAAAAACAAGTGGACCGCAAGGCGCAGCGGTTAAAGGATAAAATTGAAAGGATGAGGAGCGCTC GTGCTGTCAGCAGATGCGCGGTGGGAACCAACAAAGAAAGTCTCTCGGTTGACCACAGAAAGCCAGAAAGGAGGGAG GATGTAGAGCAACAGCAGCAGC
Tb927.9.4420	ATAATACCAATGTGATGGAT GTCCAAGTCTAGTCGTAAA TATATACCATAGAGTTGGCC CATCCAAGCCTCCAGAGGT	GTCCAAGTCTAGTCGTAAAAATCACTTGCCTATTGCCCTCCGCTTCCAACCAAAGTGCGGATAAGAGGGGAGAGCTGCAGT TGAAGAAGCAAGGACCAGGGGAGCAACCGGCCAATGAGGCTATAACGGTGCCAGATCTGAAACTAGACGAAACAGTCCGC ATAAGGGAAATGTTTACGGAGTATATTAATGGTGAGTATGTAACCACTATTTGACCTTCGCGTGCTCCCTTCAGAGCT TGGAGTATATCCCTCCGACGATGAAATGACACTTGTATGACCGCATTTGAGAACAAAGTGAGTTTTACTAATCTCTGTGA GGTACATGCGGTTTTACAAGAAAGAAATTTTGGAAATCGAACAGCAACGTCACCGTTCCAATGCCGCGCAAGATGAATGC GAGGACACGCTTCGTGCCTTTGTTTCACTTGGTGGCAACGAAGATGGAAGTGGGAGCGTCTTAGTGGAGGACTTACGGCA GGTGTGCAGAACTTCGGCCTCACTATTGATATAAACGAGGCACCTCAATGGTTTGAATGAGTCAGAGAGCCCCCTTAACGT TGCCTATATGGAATTTTGAACCTGTGGAAACATCAAAGCCGTGAGCGAGGTGGGAATCGGGAACAATACGCAGCCTT TCCTTAACCGATACCTGTATACCTCTGGAGGCTTGGATGGG
Tb927.6.3100	ATAATACCAATGTGATGGGA AGTACCAGAGACAACAGC TATATACCATAGAGTTGGTTCTG TGTTGAAAGTGTTGAT	GAAGTACCAGAGACAACAGCTCCAAATCTTGGGTACAAACACAGGAGTACGCTATGTTGAACGCCAACGCTAGTCGCGA AGTGCAGGAACTTTTTAAACGCATTCTTGATTATCAACCTCAGACACCAGAAGTCCCGCCAGCTACGTCCATTTATTC CCGACTACGTTCCCTCCATTGGCGACCTCGATCCATTCTGTAAGATTCCACGACCTGATGGCAAGCCCGACGGTCTGGGT ATATATGTGTTGGATGAACCTCTGTGGCACAATCTAATCCTGCCGTAGTCTCTACTAGAAGTTCGTGCAACAAATATTCA TTCGTTGGTGGCTTAGCGGAAGCTGTGGATTCTTTTGGAGTGCAGCAATAGACCGGAGGTGATTGATCGCTGGATAA ATGATGTGAAGAAGGTACACTATAAAAGCCTTTACCCACCATTAACTACCAAAAACCTATGCCTGAGATAGATTGCTT TTGCAAGTGTGGCCACAGGAATTCGAAGAATTCCTCAATTCGGATGTGAGTTCCCAACCCCTCAATTCGATCTTGATT GGATCAGTATGTGAGGGCTTGTGTTGATTTCTCGATATTCCCACTTATACCTCACTTATTGACTCCTTGACGTGATGT TCACGCTCTATCAGGAGTTTAGGGCAATCAACACTTTCAACACGAA

Movie S1 (related to Figure 4). High speed videomicrographs and the corresponding kymographs of different classes of *L. mexicana* flagellar movement. Four examples of flagellar (tip-to-base symmetrical), interrupted flagellar, uncoordinated/static and ciliary (base-to-tip asymmetrical) beating are shown. Cell movement due to swimming or rotation has been digitally subtracted.